Physics of inorganic upconverting nanophosphors and their relevance in applications

Maura Cesaria

Department of Mathematics and Physics "Ennio De Giorgi", University of Salento, 73100-Lecce (Italy)

e-mail address: maura.cesaria@le.infn.it

Abstract

Upconversion luminescence involves absorption of one or more low energy (commonly infrared wavelength) photons leading to emission of a high energy (i.e., visible or ultraviolet wavelength) photon. It is widely exhibited from lanthanide-doped materials with low phonon energy whereby multiple electronic transitions may occur between the f-states of the luminescent centers. Since upconversion processes require metastable and long-lived intermediate energy levels acting as storage and reservoirs of the exciting photon energy, rare earth lanthanide ions are particularly suitable due to their rich scheme of 4f energy levels poorly affected by the crystal field.

In this framework, inorganic upconverting nanoparticles (termed nano-upconverters herein), that is (sub- 20 to 100 nm) nano-sized inorganic materials exhibiting photon upconversion, have gained a lot of attention from the scientific community owing to their numerous applications (optoelectronics, nanophotonics, nanomedicine, biological and biomedical sensing and labeling, nano-thermometry in cells, photodynamic therapy, and amplified stimulated emission), advances in nanofabrication allowing nanostructured design and control on the surface composition as well as integration processing. Furthermore, remarkable differences as compared to the bulk counterpart materials due to scaled-down size, increased role played by surfaces and changes in the phonon density of states have prompted advances in the theoretical understanding of upconversion pathways and mechanisms.

This chapter provides an introduction to the physics of nano-upconverters and discusses the relevance of the associated phenomena in applications. It is overviewed the basic processes related to and leading to upconversion (excited state absorption, energy transfer upconversion, cooperative transitions and photon avalanche), the role played by rare earth ions with their ladder-like scheme of energy levels, the critical choice of the host crystal, the factors affecting luminescence quantum yield and the impact on spectroscopy of upconversion of the size-dependent changes in the phonon density of states. In this respect, the advantages in using nano-upconverters with respect to materials exhibiting quantum-size effect, the role played by increasing surface-to-volume ratio and the relationship between peculiar aspects of nano-upconverters and applications are discussed.

This chapter consists of two main sections: the first part focuses on basic knowledge on upconverters and the second one discusses the topics overviewed in the first part by pointing out the changes related to the spatial confinement. The extensive fundamental information provided in the first part makes the readership of this chapter open to non-specialist readers and lays the foundation of the needed knowledge to read the second part easily. Due to the impossibility of covering all the aspects of the physics and applications of upconversion at the nanoscale in this contribution, extensive literature sources are provided for the reader's guidance. The fascinating and still not completely understood physics of nano-phosphors is expected to be an interesting research field with relevance in applications and fundamental knowledge in the upcoming years.

Keywords: Upconversion, lanthanide dopants, spatial confinement of phosphors, engineered nanoupconverters

1. Introduction:

The worldwide scientific interest in the field of inorganic luminescent materials is documented by the huge number of publications reporting on their properties and applications. On a fundamental level, understanding the physics of such materials requires knowledge of several basic concepts in different fields, such as solid state materials, role of dopants and crystal symmetries, spectroscopy mechanisms and phonon-related processes. In this introduction paragraph, the basic definitions and concepts, nomenclature, interplay between luminescence mechanisms and properties of materials, importance of rare earth ions in upconversion processes and potentialities/changes related to the spatial confinement of upconverting materials are overviewed. The emphasis is placed on general concepts to make the readership of this paragraph open to non-specialist readers that can gain the needed knowledge to follow the subsequent discussion focusing on nanoscaled luminescent materials.

1.1 Background knowledge and nomenclature

Technically, luminescence refers to spontaneous emission of electromagnetic radiation (photons) from a material that absorbs energy from a source (external stimulus). Although the term "luminescence" was first introduced in 1888 by the German physicist Wiedemann, using the German word "luminescenz" [1], the knowledge about luminescence phenomena dates very back in the history of humans [2]. Materials exhibiting luminescence are termed luminescent materials or phosphors (light bearer in Greek) according to the term coined in the 17th century by Vincenzo Cascariolo, an Italian shoemaker from Bologna, who documented persistent luminescence in the dark following the exposure to the Sunlight of a stone (baryte) from the outskirts of Bologna [3].

Luminescence is a final result (the output) that may result from a sequence of different processes initiated by an absorption event (the input). Within the energy scheme of the element under consideration, absorption may occur as ground state absorption (GSA), that is promotion of an element from its ground state (i.e., the lowest energy state) to an excited state, or excited state absorption (ESA), that is promotion of an element occupying an excited state to an excited state with higher energy. Linear and non-linear absorption processes can be distinguished depending on the intensity of the excitation. Non-linear or multi-photon absorption is classified as "non-resonant" and "resonant" if it occurs without and with the assistance, respectively, of intermediate gap states. Non-resonant multi-photon inter-band absorption fulfills the law $I=I_o P^n$, where I is the intensity of the emission peak, P is the pumping power, I_o is a constant and n is the number of photons involved in the multi-photon absorption [4,5].

Depending on the nature of the excitation source (electromagnetic radiation, electric current, temperature, chemical reaction, cathodes, X-rays, biochemical reaction and mechanical energy), luminescence can be referred to as photo-luminescence, electro-luminescence, thermo-luminescence, chemo-luminescence, cathode-luminescence, X-ray luminescence, bio-luminescence and mechano-luminescence, where the prefix classifies the excitation source. In particular, optical excitation of luminescence refers to photoluminescence induced by absorption of ultraviolet (UV) or visible light. Photo-luminescence phenomena are classified as "fluorescence" whenever the emission time-scale is very short (10^{-9} sec < t < 10 ms) and "phosphorescence" if the emission time-scale is relatively long (t > 0.1 s up to hours or even days) [6].

In general, photoluminescence may result from the interplay between several so called "radiative" (that is, photon emitting) and "non-radiative" or" radiationless" or "phonon-assisted" transitions for which the pump energy is lost in other processes (typically heat transfer) competing with luminescence. These transitions belong to the class of the so-called multi-phonon relaxation mechanisms that refer to decay of excited electronic levels by excitation of lattice vibrations (phonons) rather than photon emission [7]. Photoluminescence is termed "resonant" if both emitted and excitation are energy matching.

The rate of radiative relaxation between two levels with an energy mismatch ΔE can be expressed according to the Judd-Ofelt theory [8,9]
.:

$$W_R\ i \rightarrow f = \frac{64\ \pi^2 \Delta E^2}{3h\ (2I_i+1)}\ \chi F^2 + n_h^3 M^2$$

where F^2 is the matrix element of the electric dipole moments, Ii is the angular momentum of the initial state, M^2 is the matrix element of the magnetic dipole moment, n_h is the refractive index of the host crystal and $\chi = n_h (n_h^2+2)^2/9$ is a corrective factor (Lorentz correction) for the local field.
The non-radiative relaxation rate W_{NR} of a transition between two states separated by the energy gap ΔE can be expressed by the following relationship [10]:

$$W_{NR}\ i \rightarrow f,T = W_0\ \frac{\exp\ \frac{h\nu_m}{kT}}{\exp\ \frac{h\nu_m}{kT}\ -1}^{\frac{\Delta E}{h\nu_m}}$$

where T is the absolute temperature, W_0 is the transition rate at T=0 K (ground state of the phonon modes), $h\upsilon_m$ is the highest fundamental phonon energy of the host lattice vibrations (phonons) coupling to the electronic transition i→ f of the element under consideration. Therefore, multiphonon transitions are favored whenever the energy mismatch ΔE is larger than the phonon energy $h\upsilon_m$ and involves phonon-assisted decay whereby multiple lattice phonons are emitted or absorbed in order to bridge the energy difference ΔE. If the phonon energy is large or the energy gap is small or a small number of phonons are required to bridge the energy gap ΔE, then the phonon-assisted transition is more probable than the radiative transition. Simple examples that illustrate how small gaps and large gaps favor non-radiative and radiative decay pathways, respectively, are provided in Figure 1. Figure 1 (a) depicts the situation of a three-level system being excited to the topmost energy level (labeled by 3) from the bottom level (labeled by 1). If the energy gap between the levels 1 and 3 is so large to make improbable a non-radiative relaxation from the level 3 to the level 1 and the intermediate level (labeled as 2) is closer in energy to the level 3 than to the level 1, then the more probable relaxation decay of the system excited in the level 3 is a radiationless transition from the level 3 to the level 2 rather than a radiative decay to the level 1.
In the case of a more complex distribution of energy levels, the possible decay transitions of an element with a discrete series of energy levels can be either radiative or radiationless depending on the energy gap between the levels involved in the transition. For instance, following photon excitation, the possible decay transitions of an element with a discrete series of energy levels can be described by the simplified representative energy-level diagram reported in Figure 1(b). Once the element is excited from the ground state (labeled as zero) to one or more of the upper lying energy levels (labeled as 3, 4, 5), if such excited states are closely spaced in energy then relaxation occurs mainly via level-by-level radiationless cascade transitions (dashed arrows) to the level 3, which has a relatively large gap with respect to the lower-energy lying levels 2, 1**,** 0. In the case of levels with large energy gap, such as the levels 3 and 2, phonon emission is less probable and radiative transitions are favored. Hence, in the situation sketched in Figure 1(b), the level 3 relaxes with photon emission to the level 2 and the levels 2 and 1 subsequently decay to the bottom level (that may be the ground state) by radiative transitions. Therefore, depending on the level-to-level energy difference, excited states decay through two main channels, i.e., a radiative relaxation (i.e., via photon emission) or a radiationless relaxation (i.e., via phonon emission).
The occurrence of loss mechanisms reducing the photoluminescence yield, naturally introduces the concept of quantum efficiency (or quantum yield) defined as the fraction of the input photons contributing to the output luminescence process [11].

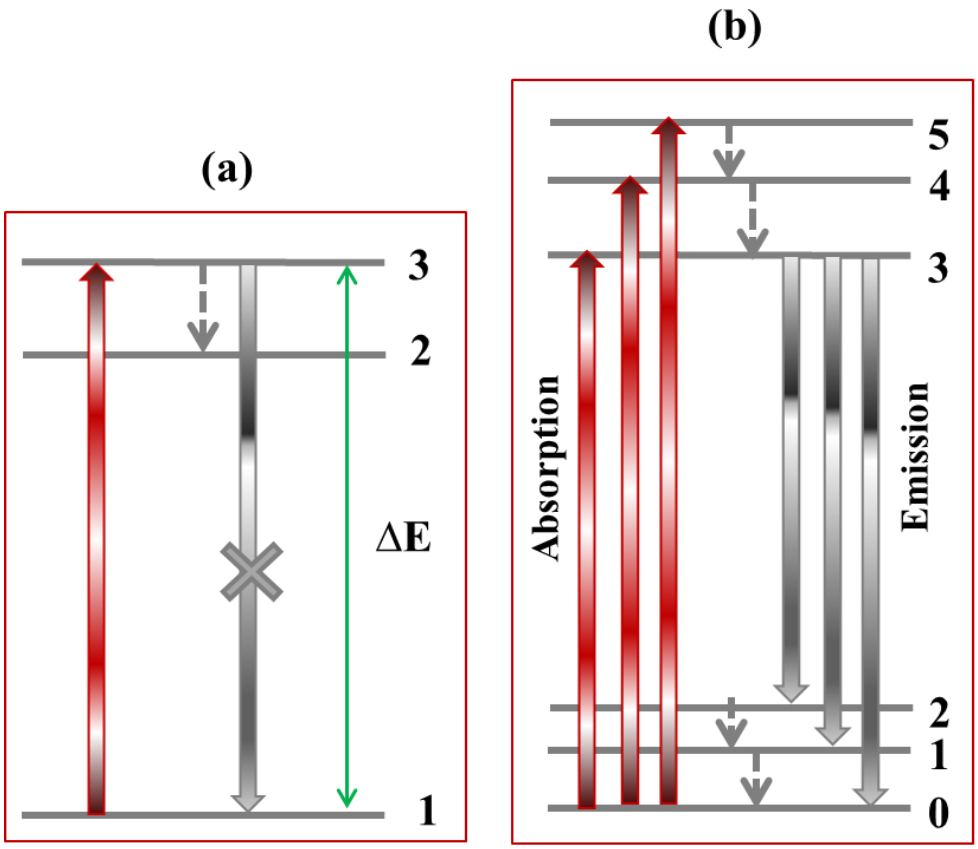

Figure 1: Examples of (a) phonon-assisted relaxation decay in a simple three level system, and (b) both radiative and ratiationless transitions occurring in a multi-level system. Absorption is indicated by upward shaded red arrows. Radiative decay is indicated by downward continuous shaded grey arrows. Phonon-assisted decays are depicted by downward dashed grey arrows.

1.2 From the Stokes principle to upconversion

The above described photoluminescence processes fulfill the "Stokes principle", meaning that the emitted photons have lower energy than the pump photons (Figure 2(a)). In this situation, the difference between the spectral position of the absorption and emission peaks related to the same electronic transition is called "Stokes shift". Also, if a thermally excited ground state is electronically excited, "anti-Stokes shift" may occur, where the energy of the radiative emission exceeds the pump energy by only a few units of k_BT (k_B is the Boltzmann's constant and T is the absolute temperature) (Figure 2 (b)). A radiative process yielding output photons with energy exceeding the energy of the pump photon by 10-100 k_BT (for instance, conversion of infrared (IR) photons to visible and UV photons) is referred to as "upconversion" .The phenomenon of upconversion luminescence through lanthanides, which is the mechanism of interest hereafter, was first observed by Bloembergen [12] via an energy diagram for crystals including ion impurities and subsequently demonstrated by Porter [13]. In practice, upconversion had scarce applications until it gained attention in the field of compact solid state lasers as an efficient non-linear excitation mechanism [14] and for the development of temperature sensors [15]. Indeed, the development of upconversion luminescent materials experienced an effective spread and interest with the advent of lasers, as demonstrated by the pioneering studies of Auzel, dating to 1960s, in which it was proposed that energy transfer pathways could involve rare earth

ions both being in an excited state at the initial step of the energy transfer rather than a first ion in an excited state an a second ion in its ground state [16,17].
Diagrams depicted in Figures 2 (c),(d) sketch the mechanisms of down-conversion (Stokes-type) (Figure 2(a)) and upconversion (Figure 2(b)) processes involving a sequence of energy levels of a luminescent center including the ground state (labeled by 0), first excited level (labeled by 1) and second excited level (labeled by 2). Phosphors re-emitting the absorbed energy at lower and higher frequency are down-converting and up-converting materials (or briefly, upconverters), respectively.
Once absorption promotes the transition from the ground state to the excited state 2, decay-down channels can be radiative (i.e., photon emitting, continuous shaded grey arrows) or radiationless (i.e., without photon emission, dashed grey arrows) in both down-conversion and upconversion situations. As the diagram representation in Figures 2(c),(d) shows, unlike absorption of one pump photon (one-step absorption) characterizing down-conversion, upconversion is a nonlinear optical process involving successive absorption of at least two low energy pump photons (multi-step absorption) via intermediate metastable (long lived) energy states.
Since the mid-1970s, growing interest in the upconversion process was catalyzed by its applicative possibilities in obtaining UV and visible emissions through sequential absorption of two or more low-energy near-IR pump photons via intermediate metastable levels introduced by proper efficient upconversion dopants [12,18-20].

1.3 Rare earth elements

Rare earths are chemical elements characterized by the progressive filling of the 4f atomic orbitals and include the elements with atomic number Z ranging from 58 to 71 (Figure 3(a)), that is scandium (Sc), yttrium (Y), lanthanum (La) and the 14 lanthanide elements (cerium (Ce) with Z=58, praseodymium (Pr), neodymium (Nd), promethium (Pm), samarium (Sm), europium (Eu), gadolinium (Gd), terbium (Tb), dysprosium (Dy), holmium (Ho), erbium (Er), thulium (Tm), ytterbium (Yb), and lutetium (Lu) with Z=71) [21]. The subset of the rare earths with electronic configuration $[Xe]4f^n5s^25p^6$ (where n = 0–14 and [Xe] refers to a xenon core) and trivalent stable oxidation state are termed lanthanides. Scandium and yttrium are classified as rare earth elements because they are present in most of the deposits of the rare earths and have similar properties as lanthanides despite their differetn electronic and magnetic properties. Whereas actinides (that correspond to filling the 5f shell from thorium (Z = 90) to lawrencium (Z = 103)) share many electronic properties of lanthanides, they may have unstable isotopes that make them less attractive optical centers than lanthanides.
On the basis of a systematic investigation of the absorption and luminescence spectra of the lanthanide series in a $LaCl_3$ crystal performed in the 1950s and 1960s, Dieke and co-workers listed the energy levels for all lanthanides in the energy range 0-40 000 cm^{-1} organized according to the Dieke's diagram [22]. Extended measurements involving the energy levels of the $4f^n$ electronic configurations of lanthanides in various host lattices demonstrated that Dieke's diagram is valid independently on the host lattice. In practice, the Dieke's energy-level diagram shows the energies of the states of the trivalent rare earth ions with the magnitude of the crystal-field splitting indicated by the width of the state and the energy location of the corresponding free ion energy level ($^{2S+1}L_J$, S and J quantum number of spin and total angular momentum) given by the center of gravity of each J-multiplet. Hence, prediction, identification or assignment of the emission lines of rare earths in listed crystals and new hosts can be easily made based on the Dieke's diagram.
A peculiarity of rare earth dopants as luminescence centers is that they emit and absorb specific wavelengths related to transitions relatively insensitive to the chemical surroundings. From the perspective of optical properties, rare earth elements can exhibit *f-f* transitions (involving ground state and excited $4f^n$ states) and *d-f* transitions (involving f^n ground state and $4f^{(n-1)}$-*5d* excited states).

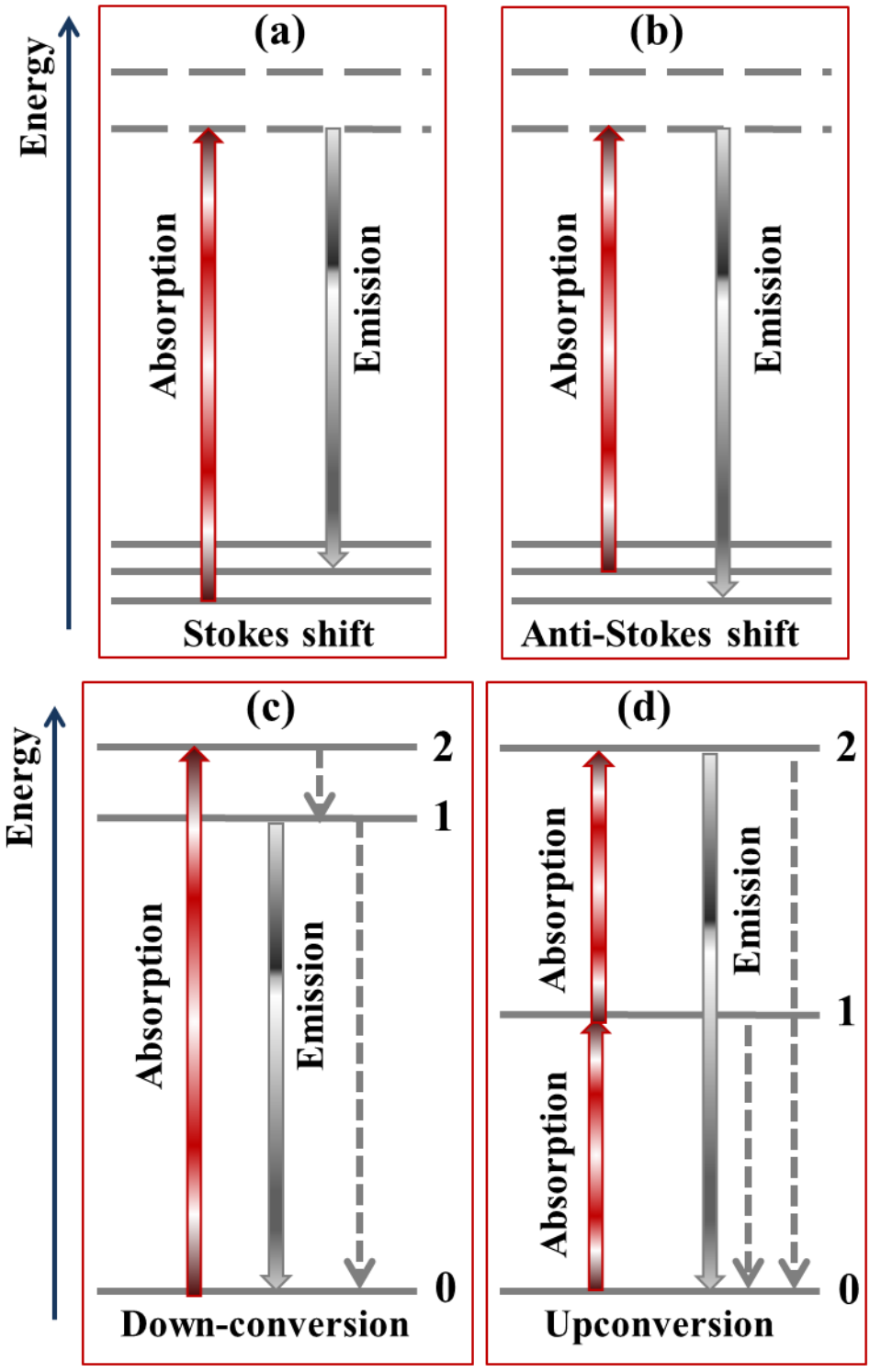

Figure 2: Sketched energy level diagram of photoluminescence occurring according to (a) the Stokes principle, (b) the anti-Stokes mechanism, (c) down-conversion, and (d) upconversion. Absorption is indicated by upward shaded red arrows. Radiative decay is indicated by downward continuous shaded grey arrows. Radiationless decays are depicted by downward dashed grey arrows.

The observed IR and visible emission spectra of lanthanides result from transitions between the *4f* states, that exhibit small host-induced splitting and mix weakly with higher energy states due to shielding by the outer *s* and *p* orbitals. Such *f-f* transitions are characterized by sharp emission lines (full width at half maximum (FWHM) < 10 nm), weak intensities, relatively poor sensitivity to the host lattice, long lifetimes of the metastable states, efficient emission, little or no vibronic structure (phonon-assisted transitions) and weak radiationless relaxation of excited states [23].

Therefore, as a consequence of the weak coupling between f–f transitions and local crystal field, lanthanides emit selectively sharp lines characteristic of the emitting source. Differently, spectroscopy of transition metal elements, characterized by partially filled *d* atomic orbitals, is strongly dependent on the crystal field as a consequence of the formation of ligand-dopant hybridized states. In general, the relationship between the electronic structure of the emitting center and the transitions allowed by the selection rules and crystal symmetry is important to understand spectroscopy of phosphors. Luminescence transitions between the electronic states of the rare-earth elements are mainly electric-dipole transitions and their selection rules are $\Delta l = \pm 1$, $\Delta S = 0$, $|\Delta L|$, $|\Delta J| \leq 2l$, where $l = 3$ for lanthanide series ions. For centro-symmetric rare earth sites, magnetic dipole transitions are allowed, i.e., the selection rule is $\Delta J = 0,1$ and when $\Delta J = 0$, any transition involving another state with J=0 being forbidden, only $\Delta J = |1|$ is allowed.

Forced dipole transitions involving states described by mixed wave functions exhibit weak intensity (directly depending on the degree of mixing) and very sharp emission peaks. Hence, although the emission lines of the *f-f* transitions are almost independent on the host lattice (chemical environment), the relative emission intensity is affected from site symmetry and selection rules [8,9].

In principle, as parity doesn't change, the transitions within *4f* shells are strictly forbidden by the Laporte's or orbital rule. This constraint implies that *f-f* transitions show a very weak oscillator strength ($\sim 10^{-6}$) and only muck weaker magnetic dipole transitions can occur in centro-symmetric crystals. Instead, *f-f* transitions are allowed for non-centrosymmetric sites: whenever a rare-earth ion occupies lattice sites lacking of inversion symmetry, mixing between states 4f with different (opposite) parity can result from rare earth- crystal field or rare earth- lattice vibrations interaction [8,24,25].

Rare earths can be also involved in inter-configuration (i.e., 4f-5d) transitions that, unlike the intra-configuration transitions, present broadband absorption and emission spectra as well as dependence on the host crystal field. They are characterized by emission lines with FWHM ranging from 30 to 100 nm and are strongly dependent on the host lattice owing to the more extended and delocalized character of *5d*-orbitals compared to *f*-orbitals. Hence, $4f^{n-1}5d$ configurations of rare earth ions in solids are very different from those of the free-ion counterparts. In the case of *4f-5d* transitions, changes in the covalence-degree of the dopant-ligand bond can induce shift of the luminescence emission due to splitting of d-levels depending on site symmetry and crystal field strength. A comprehensive report on classification and theory of the 4f-5d absorption and emission energies of divalent and trivalent lanthanides inserted as dopants in more than 1000 inorganic compounds was provided by Dorenbos [26-28]. To summarize, on comparing *f–f* and *f–d* transitions, it results weak versus strong ion-lattice coupling strength, electric dipole oscillator strength of 10^{-6} versus 10^{-1}–10^{-2}, and life-time of 10^{-2}–10^{-5}s versus 10^{-8}–10^{-6}s.

From the standpoint of upconversion, direct excitation of lanthanides is usually an inefficient process because of low absorption cross-sections and long luminescence lifetimes of the f-f transitions. On the other hand, since most inorganic crystals are not able to work as upconverters at room temperature, lanthanide dopants have to be inserted in well selected crystalline hosts to observe efficient upconversion luminescence and tunable multi-color emission [18,29].

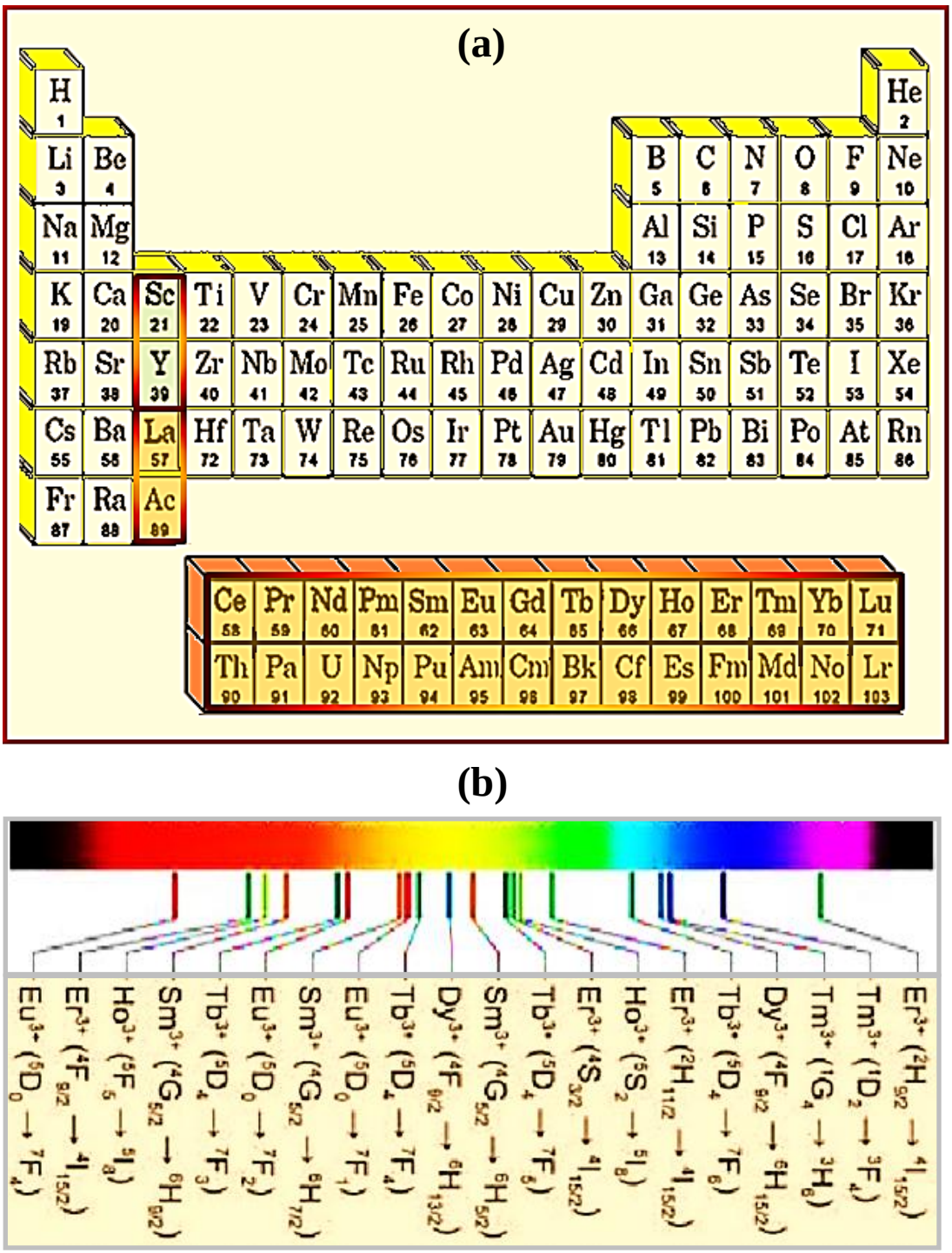

Figure 3: (a) Periodic table of the elements showing the rare earth end lanthanide series. (b) Diagram showing the richness of color output from the main f-f transitions of rare earths.

Basically, lanthanide elements are particularly suitable to be exploited in upconversion processes for two main reasons. First, they have multiple spectroscopically active atomic-like levels ideal for selective color output (Figure 3(b)), mixing of different color output and energy transfer between discrete levels of the same as well as different ions. Second, with the exception of Yb^{3+} and Ce^{3+}, lanthanides have metastable (i.e., parity-forbidden but partly allowed in optical transitions) energy levels with lifetimes in the microseconds to millisecond range. Due to their slow decay, such long-lived levels are able to accumulate transient population, hence acting as storage and reservoirs of the excitation photon energy. In regard to the host matrix, sodium rare-earth fluorides $NaREF_4$ (where RE=Y, Lu, Ga) are chemically stable efficient materials due to low photon energy that favors increased upconversion quantum yield by decreased probability of phonon-assisted decays [30,31]. Basically, to enhance the upconversion emission efficiency of rare earth ions, a proper choice of host and dopant–dopant pair (the so called activator-sensitizer pair, as it will be detailed hereafter) is needed due to several disadvantageous factors, such as small absorption cross section of rare earth ions due to parity-forbidden 4f-4f transitions and non-radiative relaxations taking place simultaneously with upward transitions in the presence of closely spaced levels.

Investigation of fundamental and practical applications of phosphors and, in particular, upconverters has experienced a speed up and renewed scientific interest recently due to the advancement in synthesis methods and processing of nanomaterials combined with the requirements/opportunities of integration [32-34]. Inorganic upconverting nanoparticles, that is sub- 20 to 100 nm nano-sized inorganic materials exhibiting upconversion, show peculiar behavior and properties, related to or modified by the spatial confinement, that are very sensitive to nanoparticle size, crystal phase, doping content, distribution and density of defects, surface-to-volume ratio. Indeed, on turning from bulk- to nano-scaled materials additional effects play a role in affecting the luminescence and upconversion emission efficiency stemming from the increasing importance of surface and confinement-related changes, as it will be discussed hereafter. For instance, practical spectroscopic applications of upconverting nanocrystals have to face the drawbacks of limited quantum efficiency and luminescence quenching caused by increased density of surface weakened bonds and bonded activators [35]. Moreover, a reduction in size implies a decrease in the number of emitting dopant centers and enhancement of surface quenching effects that can either complicate energy transfer pathways between the energy levels of lanthanide ions or favor defect-promoted radiationless transitions. All of this makes clear that a fine control on the synthesis is demanding to ensure efficient size-dependent luminescence and to advance in the theoretical understanding of the differences with respect to the bulk counterpart materials resulting from scaled-down size [36-39]. Hence, in parallel to careful nanofabrication [34], to fully exploit the opportunities offered by upconverting nano-scaled phosphors (briefly termed nano-upconverters, hereafter) and ensure high quantum yield in biological applications preferring particles smaller than 20-30 nm, fine control on phase, concentration of lanthanide dopant and co-doping, surface chemistry, particle size and size dispersion, energy transfer losses between dopants and defects is demanding [39,40]. In this respect, design strategies yielding both chemically and structurally engineered nanocrystals are also critical to solve for the above mentioned drawbacks through modification of the energy transfer and upconversion pathways, surface passivation, pumping scheme, core-shell design, coupling to surface plasmon modes and photonic crystals [41-44].

In view of the already extensive literature dealing with phosphors, the intent of this chapter is to overview the physics of phosphors in the spirit of pointing out the fascinating and still not completely understood behavior and challenging properties of nanoscale-sized materials acting as upconverters. In this context, the emphasis placed in the introduction on basic definitions, nomenclature, radiative and radiationless building-block mechanisms, importance of rare earth ions in luminescence is essential to make the readership open to non-specialist readers and provide to a reader, new to the field of luminescent materials, the needed knowledge to gain curiosity on the fascinating and still not

understood field of upconverting nanomaterials. A preliminary and/or complementary reading of Refs [23,45] can be useful to the reader to cover aspects mentioned and not developed in this contribution.
The chapter develops in two main sections. The first part focuses on basic physics of phosphors, concepts of activator and sensitizer, interplay between dopants depending on doping level and energy level scheme, dopant-dopant interaction mechanisms involved in the main upconversion processes. The second part of the chapter develops and extends the topics related to nanomaterials overviewed in the above preliminary introduction by pointing out the changes related to the spatial confinement in comparison with bulk upconverters. Several examples as well as recent applications of upconversion in the framework of nanomaterials are discussed. Due to the impossibility of covering all the aspects of the physics and applications of upconversion at the nanoscale in this contribution, extensive information on the literature is provided for the reader's guidance.

2 Inorganic phosphors: hosts and dopants

According to a literature survey, inorganic phosphors can be categorized in three main classes depending on their composition: the first class includes thermally and chemically stable crystals embedding luminescent centers as stoichimetric components, the second class consists of optically inactive materials (usually termed host crystals) doped with proper concentration and kind of luminescent ions (activators, sensitizers, activator-sensitizer pairs as it will be discussed), and defect-related luminescent materials emitting for a specific concentration of defect and/or reaction conditions belong to the third class.
Luminescent pure lanthanide oxides, such as Eu_2O_3 and Tb_2O_3, are examples of phophors whereby luminescent centers (Eu^{3+} and Tb^{3+}) are stoichimetric components. The onset of radiationless self-quenching processes related to the concentration of the luminscent centers makes them not particularly efficient phosphors [46].
Turning to the other classes of phosphors, the choice of a host matrix is as crucial as the choice of dopants: while the energy-levels ruling radiative and radiationless transitions depend on dopants, the host not only provides the doping sites for the luminescent centers but is also responsible for the chemical environment (ligand-dopant bonding), coordination number of dopants, dopant-to-dopant distance and relative positioning, dopant-ligand coordination and site symmetry.
Although transition metal and actinide ions are also capable of upconversion [20], the fact that lanthanide- ligand bonds are more ionic than transition metal-ligand bonds implies a larger number of possible coordination numbers for lanthanides than for transition metals as well as more symmetries [47]. Doping can lower crystal symmetry by combining the same oxidation state with different ionic radius or dopant site symmetry in different host phases and lattice site.

2.1 Host crystals

Suitable host materials for upconverion are fluorides (i.e., sodium yttrium fluoride ($NaYF_4$), lithium yttrium fluoride ($LiYF_4$), sodium lutetium fluoride ($NaLuF_4$), calcium fluoride (CaF_2)), lutetium orthophosphate ($LuPO_4$), lutetium borate ($LuBO_3$), vanadium yttrium oxide (YVO_4), zirconium oxide (ZrO_2), yttrium oxide (Y_2O_3), gadolinium dioxide (Gd_2O_3). Tungstate, molybdate, and vanadate compounds let indirect excitation of rare earths through energy transfer processes from the host. Since such mechanism is more efficient than direct excitation of rare earths, efficient luminescence and high brightness can be obtained.
As general guidelines, in order to favor efficient upconversion luminescence host lattices have to fullfill a few key requests: i) close lattice matching with dopant ions to control lattice distortion, ii) low phonon energies to improve the emission efficiency and reduce non-radiative losses according to the multiphonon relaxation rate expressed by the exponential energy-gap law of Van Dijk and Schuurmans [48], iii) transparency to both excitation radiation and upconversion emission (oxides, nitrides, and

sulfides are wide gap host matrices fullfilling such transparency constraints), and iv) asymmetrical crystal field leading to mixed parity states [49].

In regard to point i), changes in the volume of the unit-cell resulting from substitution of a host-ion by a rare earth dopant can imply changes in the strength of the crystal-field around the dopant that shift its emission energy. Inorganic compounds of trivalent lanthanides are a natural choice as host for rare earth dopants. For instance, in the case of $NaYF_4$ working as host crystal, the residual difference between the ionic radius of Y^{3+} and both Yb^{3+} and Er^{3+} implies poor lattice distortion in Yb^{3+}-Er^{3+} co-doped $NaYF_4$, which is a very efficient upconverter. Other elements with ionic size close to lanthanides are alkaline earth ions (Ca^{2+}, Sr^{2+}, and Ba^{2+}) and transition metal ions such as Zr^{4+} and Ti^{4+}.

Turning to point ii), whereas the energy level structure of lanthanide ions is relatively insensitive to the chemical background, phonon density of states play a key role in radiationless multi-phonon relaxation transitions between closely spaced lanthanides' levels. On the basis of the energy gap law [10,48], unlike high lattice phonon energies that may quench excitation, low phonon energies yield enhanced upconversion efficiency by decreased relaxation rate. Indeed, host matrices with low phonon energy can drastically influence the competition between phonon-related and radiative processes, hence impacting on the upconversion luminescence properties [50]. A guiding rule can be individuated on the basis of the multiphonon relaxation rate expressed by the exponential energy-gap law of Van Dijk and Schuurmans

$$W_0 = C \exp\left(-\alpha \frac{\Delta E}{h\nu_m}\right)$$

where C and α are parameters characteristic of the host crystal and $h\upsilon_m$ is the highest phonon energy of the host that couples to the electronic transition between levels with energy spacing ΔE [48]. The occurrence of multi-phonon processes therefore depends on both the host material and the electronic structure of the involved levels. For a number of phonons larger than two, the logarithm of the multi-phonon decay rate decreases linearly with the above defined energy gap, i.e., with the number of phonons bridging the gap [47].Therefore, host crystals having low phonon energy $h\upsilon_m$ decrease the probability of radiationless relaxation channels, which is beneficial to improve the luminescence efficiency. The phonon energy involved in energy transfer and upconversion pathways is lattice-dependent [51].

Fluorides have attracted attention as host materials due to their low phonon energy (~350 cm^{-1}). Hexagonal phase $NaYF_4$ doped with Yb^{3+}/Er^{3+} pairs is a very efficient upconverter under excitation at 980 nm. Also, over-performing upconversion results from the $NaLnF_4$ (Ln = La, Y, Lu, Gd) and LnF_3 fluorides [52].

As a further example, trivalent Eu^{3+} ion is a red-emitting dopant ($^5D_0$–^7F_J transitions, where J = 0, 1, 2, 3, 4) that shows low efficiency emissions from the higher-energy ^5D levels ($^5D_1$ (green), $^5D_2$ (green, blue), and $^5D_3$ (blue)) depending on phonon frequency and crystal symmetry of the host lattice as well as doping concentration. The low phonon frequency of fluoride and oxyfluoride crystals makes them suitable hosts for Eu^{3+} [53]. On the other hand, under low doping level (x = 0.008, 0.015), the probability of emission from the excited $^5D_{0,1,2,3}$ levels of Eu^{3+} is larger in $CaIn_2O_4$ than in Y_2O_3 as a consequence of a vibration frequency of 475 cm^{-1} for $CaIn_2O_4$ and 600 $cm^{-1}$for Y_2O_3 [54].

In comparison with fluorides, whereas oxides exhibit better thermal and chemical stability as well as mechanical strength, non-radiative losses makes the upconversion efficiency/brightness lower for oxides than for fluorides. About oxides and halides exploited as host materials for upconverters, stability is another critical issue. In the case of oxides, air stability coexists with not efficient upconversion luminescence due to large phonon energies. Differently, phonon energies of halides are small (< 350 cm^{-1}), which is favorable to high upconversion efficiency, but such hosts are unstable in air and sensitive to moisture [55]. Phonon energy intermediate between oxides and halides is exhibited

by ZnS, that, being very stable in air, is a valid alternative for upconversion ($ZnS:Mn^2$ is an example of upconverter).
In regard to the impact of lattice symmetry, luminescence may be phase-dependent [29]. For instance, as the site symmetry of Er^{3+} dopants is reduced turning from the O_h symmetry of cubic $NaYF_4$ to the C_{3h} symmetry of hexagonal $NaYF_4$ and from the D_{4h} symmetry of tetragonal ZrO_2 to the C_{2h} symmetry of monoclinic ZrO_2 [19], the upconversion luminescence of Er^{3+} is 10 times brighter as a result of changed transition probability. Besides lowered site symmetry, shifting of the energy levels and phonon energy can affect the upconversion luminescence too [56]. For example, due to low phonon energy, hexagonal phase NaYF4 is a very efficient upconverter despite lanthanide dopants occupy a high symmetry crystalline site [56].

2.2. Activator and sensitizer ions

In general, luminescence phenomena in phosphors result from a number of processes involving interaction between dopant centers termed "sensitizer" (in brief, S), which is the ion directly excited, and "activator" (in brief, A), which is the ion receiving energy from the sensitizer and yielding luminescence. Hence, the simplest scheme is a two-ion sensitizer-activator interaction whereby a sensitizer provides the energy levels bridging energy trasfer to the emitting activator center. Commonly, sensitizer and activator ions are termed donor and acceptor, respectively, to refer to their acting as donor and acceptor of energy.
Basic processes involving a sensitizer-activator pair, where ions can be identical and the sensitizer is in its ground state, are represented in Figure 4: radiative energy transfer (Figure 4(a)), nonradiative energy transfer (Figure 4(b)), and multiphonon-assisted energy transfer (Figure 1(c)).
The former process refers to a situation whereby energy transfer is radiative: the sensitizer (referred to as S in figure) decays radiatively and the emitted photon is absorbed by an activator (referred to as A in figure) in its ground state that gets promoted to an excited level. The probability associated with such process can be expressed as follows [20]

$$\rho_{SA}\ R = \frac{\sigma_A}{4\pi R^2 \tau_S} \int g_S(\upsilon)\, g_A(\upsilon) d\upsilon$$

where σ_A is the absorption-integrated cross-section, R is the activator-to-sensitizer distance, τ_S is the sensitizer lifetime and the integral accounts for the spectral overlap between A and S. As ρ_{SA} scales as R^{-2}, resonant radiative transfer may allow long-range energy diffusion between identical ions
For nonradiative energy transfer, the excitation migrates from one ion to the other before it may decay radiatevely and the ion-ion interactions are Coulomb interactions of the van der Waals type [57]. The transfer probability can be expressed as follows

$$\rho_{SA}\ R = \frac{1}{\tau_S} \left(\frac{R_o}{R}\right)^6$$

if both transitions are electric dipole allowed transitionsm Ro being the critical transfer spacing (i.e., equal probability of excitation transfer and spontaneous deactivation). For electric multipole interactions, the transfer probability is given by the relationship

$$\rho_{SA}\ R = \frac{1}{\tau_S} \left(\frac{R_o}{R}\right)^s$$

where s is a positive integer with the following values: s= 6 for dipole-dipole interactions, s=8 for dipole-quadrupole interactions, s=10 for quadrupole-quadrupole interactions.Noteworthy, in the case of dipole-dipole interactions, three criteria distinguish radiative and nonradiative resonant transfer. First, for radiative transfer there is no critical concentration-dependent R_o.

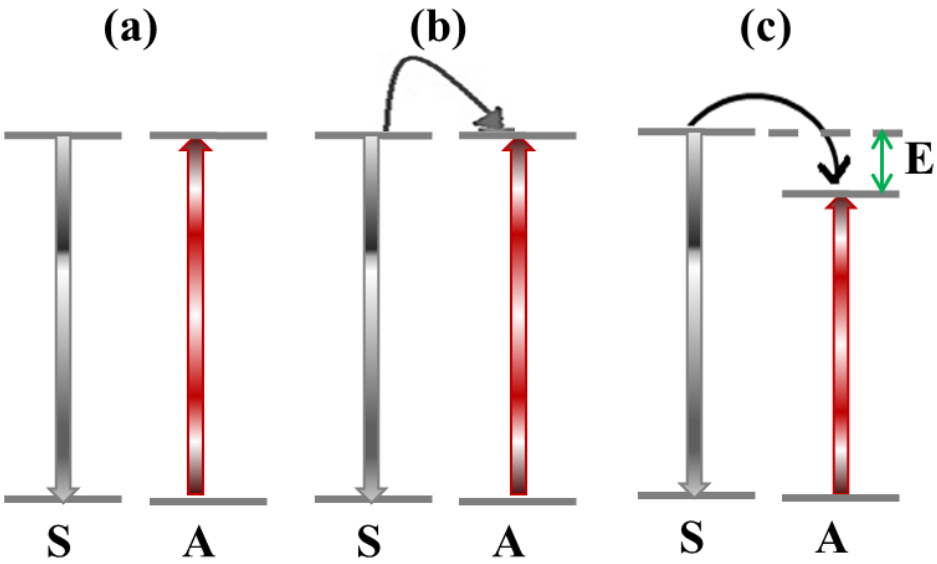

Figure 4: Basic sensitizer (S)-activator (A) energy transfer processes whereby the sensitizer in its ground state: (a) radiative energy transfer, (b) nonradiative energy transfer, and (c) multiphonon-assisted energy transfer.

Second, the transfer probability varies as R^{-2} and R^{-6} for radiative and nonradiaitve process, respectively. Third, the sensitizer lifetime does not depend on the distance R for the radiative transfer.
Unlike nonradiative energy transfer, multiphonon-assisted energy transfer involves two ions with excited states having an energy mismatch E at least of 100 cm^{-1} [58]. Being such energy gap much smaller than the energy mismatches exhibited by rare earths, multiphonon emission have to be considered while dealing with luminescence processes of rare earth doped hosts. Up to 1966 all the identified energy transfer processes between rare-earth ions were classified according to the schemes reported in Figure 4. Differently from this picture, Auzel proposed to consider activators being already in an excited state [16,17], leading to upconversion by energy transfer as a generalization to the case where the activator is in a metastable state rather than in its ground state. These processes and their implications in term of luminescence will be discussed later in detail.
In regard to more complex processes occurring in lanthanide–doped hosts, two main classes can be individuated: sensitization by the host lattice (Figure 5(a)) and transitions involving dopants being an activator (A) (Figure 5(b)) and a sensitizer" (S) (Figure 5(c)) [59].
Sensitization by the host lattice (Figure 5(a)) involves band-to-band photon absorption that generates electron-hole pairs (typically excitons under UV excitation) followed by relaxation of conduction electrons to donor levels ("D" label) and transfer of holes to acceptor states ("A" label) driving radiative emission by levels of the donor-acceptor pair. In the absence of participation of the host material in emission, luminescence involving discrete energy levels of emitting centers can occurs according to two different situations. First, an activator dopant element (label A) gets excited to a state A* by energy absorption and then emits radiatively through a down-conversion decay pattern (Figure 5(b)). Second, the desired radiative emission from an activator element can be induced indirectly by energy transfer to the activator from a nearby sensitizer turned in an excited state (Figure 5(c)).

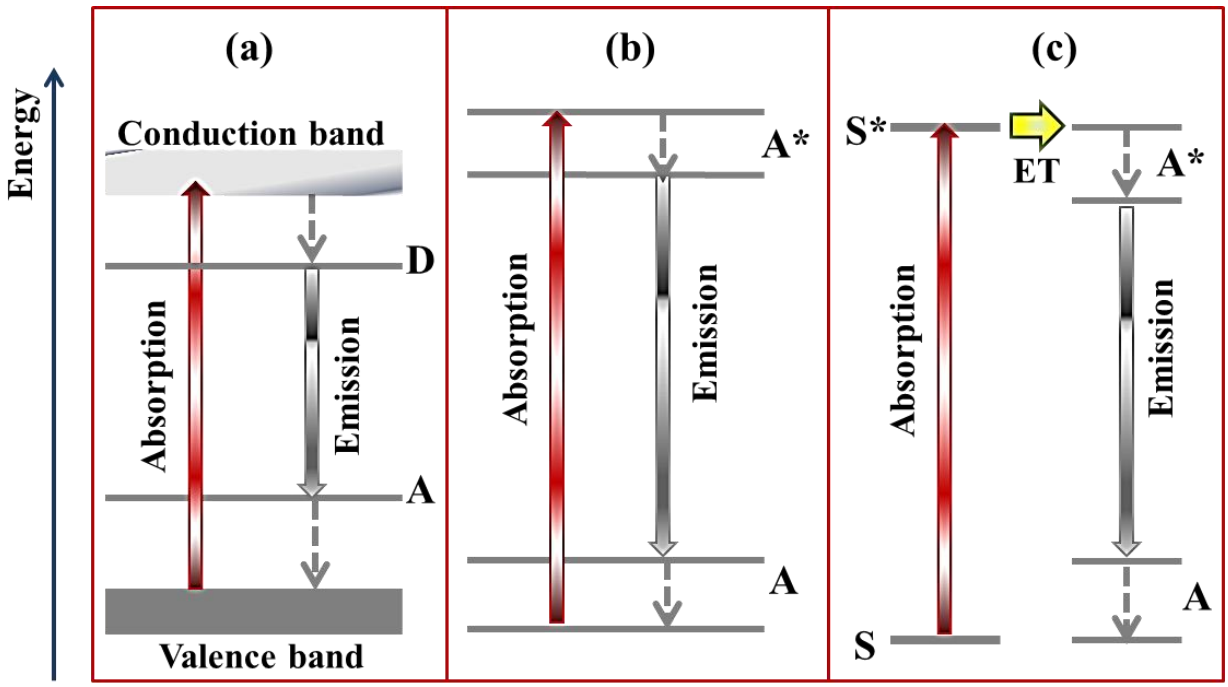

Figure 5: (a) Sensitization of the host lattice involving energy levels of foreign ions labeled by A (acceptor) and D (donor). (b) Excitation by absorption of an activator element (A) to its excited state A* and subsequent radiative emission through down-conversion. (c) The energy absorbed by a sensitizer S turned to its excited state S* is transferred to an excited state of a nearby activator dopant (A*) that emits radiatively. Dashed lines refer to non-radiative energy relaxation transitions.

The probability of energy transfer is favored by a large overlap between the wave functions of activator and sensitizer, a short intrinsic decay time of the sensitizer, a large absorption strength of the activator, and a short distance between the sensitizer and activator (the energy transfer rate drops very quickly for activator-to-sensitizer spacing greater than about 1 nm).

3. Building-block ion-ion interaction mechanisms

Several ion-ion interaction mechanisms (stepwise photon excitation, energy transfer and energy sharing, cross-relaxation, nonlinear collective processes) play a role in upconversion by rare earth activated phosphors under increasing concentration of the active ions. The existence of various pathways leading to upconversion luminescence is favored by the richness in the energy levels of lanthanide ions. Activator-activator and activator-sensitizer interactions may take place through multi-step processes including the building-block ion-ion fundamental interaction mechanisms illustrated in Figure 6(a): from left to right, two-photon excited state absorption (2-ESA), two photon absorption (TPA), resonant and radiationless energy transfer (ET), and cross-relaxation (CR).

For 2-ESA, which involves a single atom, two pump photons are absorbed by successive GSA and ESA processes involving an intermediate energy state being usually a real long-lived state. That is, if the energy of the pump photon matches the energy associated with the transition from the ground state to an excited state of an ion, this ion is promoted to such excited state (GSA transition) and, by absorbing a further photon, can be excited to a proper higher-energy-lying state through an ESA transition. The presence of metastable excited states is important to enable that single excited ions may sequentially absorb a second photon of suitable energy at comparatively low excitation densities and be

promoted to an higher excited state. Following GSA and ESA transitions, the emitted photon has larger energy than the excitation photon, hence leading to upconversion luminescence. In general, at least two photons are required and similar processes involving more than two pump photons are termed N-step ESA, where N refers to the number of stepwise absorbed pump photons. If the energy gaps between three or more subsequent energy levels of a single ion are very close in energy, sequential excitation (multi-step photon absorption, where each step requires the same photon energy) to a highly excited state can be obtained by exploiting monochromatic low energy pump source.
Two or multi-step ESA processes are single ion processes. Although the absorption transitions involved in ESA are mainly electronic transitions, they can be phonon-assisted transitions. Going from 2-ESA to TPA, the absorption of two photon occurs via an intermediate level that, unlike the intermediate level involved in the 2-ESA process, is a virtual rather than real level.

3.1 Energy transfer

Energy transfer is a particularly important process in rare-earth activated phosphors because, f-f transitions being parity and commonly spin forbidden, lanthanide ions have long-living excited states suitable for energy transfer that favor efficient upconversion luminescence. Basically, energy transfer may take place between identical centers or between two different centers (an activator-sensitizer pair) with matched energy levels and refers to a situation whereby the decrease of energy of a center causes the excitation of a neighboring center (Figure 6(a)). Following absorption of pump photons, resonant energy transfer by a sensitizer-activator pair transfers the excitation energy of the sensitizer to a nearby activator ion being in its ground state or in an intermediate state. Hence, radiative energy transfer yields photon emission from one emitter and subsequent absorption of the emitted photon by another ion, that is energy transfer transitions whereby the change in the electronic energy on the donor ion equals the change in the electronic energy on the acceptor ion. Resonant energy transfer transitions, can be classified as: i) multipolar interaction if both transitions are electric dipole transitions, ii) exchange interaction, if ion-ion spacing lets their electronic wave functions overlap and iii) (multi)phonon-assisted energy transfer, if the energy difference between the energy transfer energies is compensated by either phonon emission or absorption [59,60]. Hence, generally, energy transfer processes can occur if the energy differences between ground and excited states of sensitizer and activator are equal (resonant energy transfer) and if either a short-range exchange interaction or longer-range multipolar interaction acts. Non-radiative energy transfer between a sensitizer and an activator can stem from either electrostatic interaction (that is active over a long-range (10-100 Å)) or exchange interaction (that is active over a short-range (<10 Å)) [61,62]. Exchange interactions are favored by high concentration of the centers, large overlap between the electronic wave functions of sensitizer and activator, short intrinsic decay time of the sensitizer, large absorption strength of the activator, and a short (< 0.5 - 1 nm) sensitizer-to-activator spacing. From the theoretical standpoint, long-distance and short-distance non-radiative energy transfer can be described by means of the dipole–dipole Förster mechanism and Dexter exchange coupling mechanism, respectively. Electric multipole rather than dipole–dipole (i.e., approximation that donor and acceptor are point dipoles) interactions have to be considered when the ion-ion spacing is comparable with their size [20,62].
The Förster energy transfer mechanism works according to a very simple scheme: the sensitizer decays nonradiatively from an excited state to its ground state while an activator in its ground state is promoted to an excited state corresponding to the relaxation energy of the sensitizer ion. The Dexter exchange coupling mechanism consists of electron exchange between a sensitizer-activator pair leading to a spin-conserved singlet–singlet (that can stem from both exchange and electrostatic interactions) or triplet–triplet (that can originate from an exchange interaction) energy transfer [20,63].
In the case of sensitizer and activator ions interacting electrostatically without energy mismatch, the non-radiative energy transfer rate W_{SA} can be expressed in the framework of the Förster-Dexter model

by the simplified relationship $W_{SA}= W_S (R_o/R)^s$, where $W_S=1/\tau_S$ is the inverse of the lifetime of the excited state of the donor ion, R is the sensitizer-activator (average) spacing, R_o is the Förster radius (i.e., the distance at which W_{SA} is equal to the probability of spontaneous deactivation W_S), and s = 6 for dipole–dipole interactions, s = 8 for dipole–quadrupole interactions and s = 10 for quadrupole–quadrupole interactions [20,61,62].

In the case of the dipole–dipole Fo¨rster mechanism (s=6), experimental spectroscopic evaluation of R_o indicates that R_o^6 depends on the spectral overlap integral J given by the emission spectrum of the sensitizer and the absorption spectrum of the activator [20,63,64]. Since the probability of the Förster energy transfer is proportional to J/R^6 and decreases rapidly for $R>R_o$, enough concentration of ion-ion pairs, below the threshold favoring concentration quenching, is needed for promoting efficient sensitizer lifetime. Experimentally, a linear dependence of the energy transfer rate on the activator concentration was reported [20,65]. In the presence of high enough concentration of the donor center, donor-to-donor energy transfer may occur, that is the excitation energy may migrate among the closely spaced donors until reaching a donor close enough to an acceptor center to complete the donor-acceptor energy transfer process. Therefore, the Förster dipole-dipole energy transfer interaction is a dominant energy transfer mechanism having importance depending on the doping content due to falling down of such interaction according to the inverse of the sixth power of inter-ion distance.

In the case of energy transfer via the Dexter mechanism, the probability for the process is proportional to the spectral overlap J and decays exponentially with the distance R according to the law exp (-2r/L), where L is the sum of the van der Waals radii of the sensitizer and activator ions [62]. Hence, the smaller the energy gap between the excited states of sensitizer and activator, the greater the energy transfer rate due to increasing spectral overlap value [20].

Whenever an energy difference exists between the energy levels of the sensitizer and activator ions (Figure 6(b), right panel where $E_1 \neq E_2$), energy transfer may occur by means of radiationless phonon-assisted processes (phonon assisted energy transfer, usually referred to by the acronym PAT) if the energy mismatch can be compensated by simultaneous emission or absorption of phonons by the host crystal [66]. Under this situation, according to the Miyakawa-Dexter theory, the energy transfer rate is given by $W_{SA,PAT}(\Delta E)= W_{SA,PAT}(0) \exp(-\beta(\Delta E)$, where ΔE ($\Delta E=E_1+E_2$ in Figure 6(b)) is the energy mismatch between the levels of the sensitizer-activator pair, $W_{SA,PAT}(0)$ is the energy transfer rate without in the absence of energy mismatch, and β is a parameter depending on the strength of electron-lattice coupling and nature of the phonon participating in the PAT process [7,67,68].

Turning to energy transfer involving lanthanide ions, it can be described by the Förster dipole–dipole interaction mechanism for several reasons. First, ion-ion distance larger than a few nanometers and shielding of the f shells by the outer shells rule out orbital overlap of the f electron states that would allow the Dexter energy transfer mechanism [20]. Moreover, the occurrence of metastable states in the energy level structure of many lanthanides, random energy migration according to the Förster mechanism favors energy migration and excitation of the emitting activator center or excitation due to interactions among the neighboring lanthanides. On the other hand, the probability of energy transfer being dependent on the sensitizer-activator distance and overlap spectral integral, the overlap spectral integral is finite in the case of sharp emission and absorption of f levels and tends to zero in the presence of an energy mismatch larger than a few phonon energies of the host lattice (Dexter mechanism). Noteworthy, the weak crystal field splitting of energy levels of lanthanides results in a slight broadening of their emission and absorption spectral range. Therefore, nonradiative energy transfer with resonantly matched emission and absorption is more probable [20,36], resulting in not negligible contribution of concentration-dependent, radiationless energy transfer processes to photon upconversion.

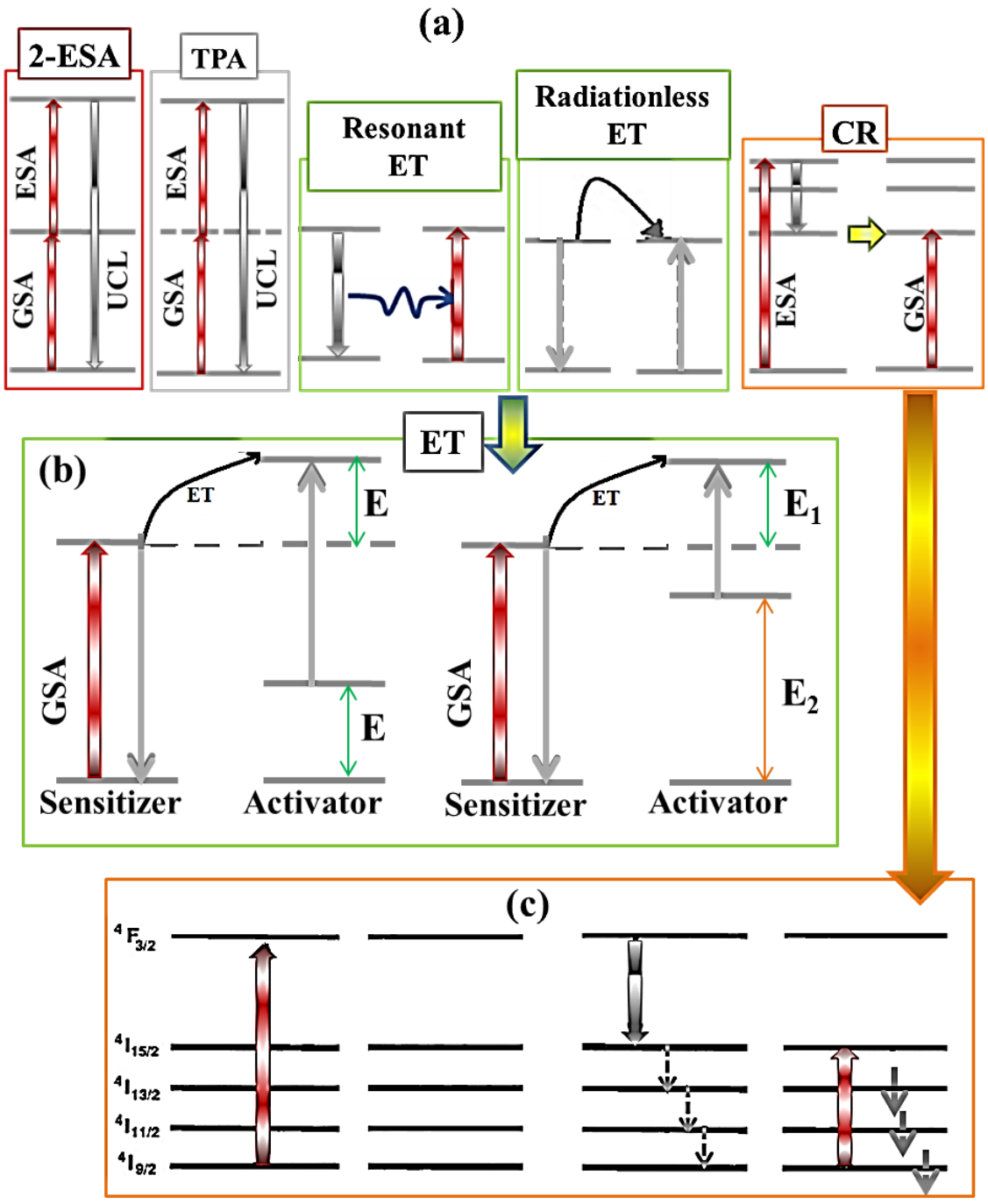

Figure 6: (a) From left to right, two-photon excited state absorption (2-ESA), two photon absorption (TPA), resonant and radiationless energy transfer (ET) between ions with matching energy gap, cross-relaxation (CR). (b) Energy transfer (ET) transitions involving sensitizer - activator pair with energy matching (left panel) and energy mismatching (right panel)levels. (c) Example of a cross relaxation process : a Nd-Nd pair

When a resonant radiative energy transfer transition occurs (Figure 6 (b), left panel where $E_1=E_2=E$), the transfer efficiency depends on how efficiently the sensitizer emission excites the activator fluorescence as well as on the spectral overlap between the sensitized emission and the activator absorption. For instance, although upconversion can be obtained by a single dopant (for example by Er^{3+} activator ion), enhanced upconversion luminescence can result from using a sensitizer (for example Yb^{3+}) to enhance the near-IR absorbance.
Noteworthy, energy transfer between rare earth ions may be either advantageous or deleterious. For instance, while $Yb^{3+} \rightarrow Er^{3+}$ energy transfer lets improve the pumping efficiency of solid-state laser devices [69], in contrast, $Er^{3+} \rightarrow Er^{3+}$ energy transfer is a loss mechanism for fiber amplifiers at 1500 nm [70].

3.2 Cross-relaxation

Among ion-ion energy transfer processes, cross relaxation promotes the acceptor ion, in an excited state or in its ground state, to a higher energy state at the expense of the donor ion that decays to a lower energy state. Cross relaxation is a radiationless process in which an ion, raised to an excited state, decays to a lower energy state E by losing an energy amount ΔE while another center is promoted to an excited state by absorbing the energy ΔE (Figure 6(a)). That is, the occurrence of a cross relaxation pathway requires that both donor and acceptor ions have two approximately energy matching levels. Following a cross relaxation event the decrease of energy of a center is associated with the excitation of another neighboring center. For instance, an excited ion may transfer part of its excess energy to another ion leading to a final energy configuration where both ions occupy an intermediate energy level. Therefore, cross-relaxation can be exploited to raise a ion to an excited state by ion-ion interaction rather than photon absorption. The two ions involved in cross relaxation may be like centers (meaning that energy migration takes place without energy loss) or unlike centers with energy matched levels (i.e., two pairs of energy levels having the same energy spacing). Since cross relaxation is a mechanism to transfer excitation, in the case of identical levels (for instance sensitizer ions), energy migration can occur without energy loss or by self-quenching under energy loss or change of the emitted photons. In the presence of an energy mismatch between sensitizer and activator, such energy gap may be compensated for by the absorption and emission of phonons. In this case the cross relaxation process is referred to as "phonon assisted". Therefore, for a pair of ions, the energy gap may be equal or matched by one or more phonons.
The working principle of cross relaxation can be clearly illustrated by the example depicted in Fig. 6(c) that refers to a Nd^{3+}-Nd^{3+} pair. Once one Nd^{3+} ion is excited to the metastable $^4F_{3/2}$ level, it interacts with a nearby like ion in the ground state (Fig. 6(c), left panel) by transferring part of its energy. As a result, both Nd^{3+} ions turn in the intermediate $^4I_{15/2}$ state (Fig. 6(c), right panel). Since the energy gaps to the lower-lying energy states are small, both ions decay non-radiatively to their ground state. Therefore, the original excitation energy is converted into heat in a short time-scale with respect to the radiative lifetime under high rate of energy transfer. A distribution of different cross relaxation rates results from Nd^{3+} ions arranged with different relative spacing. Hence, since one excited Nd^{3+} ion is required for cross relaxation, luminescence quenching (i.e., loss of radiative efficiency) changes according to a non-exponential law and is independent on the pump power [71].
As a further example, in Er^{3+}/Tm^{3+}co-doped upconverters, cross relaxation takes place in the intermediate states of Er^{3+} by means of two cross relaxation channels ($^2I_{11/2} + {}^2H_{11/2}$-$^4I_{13/2} + {}^4F_{3/2}$ and $^4F_{7/2} + {}^2H_{11/2}$-$^2H_{9/2}(^2G_{9/2}) + {}^4F_{9/2}$) that weaken green emission from $^2H_{11/2}$ and $^4S_{3/2}$ to the $^4I_{15/2}$ ground state and enhance red emission from $^4F_{9/2}$ and blue emission from $^2H_{9/2}$[20,72]. Moreover, in $Yb^{3+}/Ho^{3+}/Ce^{3+}$ triply-doped hexagonal-phased $NaYF_4$ crystal, the parity allowed *4f-5d* transitions of

Ce^{3+} ions can depopulate the $^5F_4/^5S_2$ green emitting states of Ho^{3+}while populating the $^5F_2$ red-emitting level of Ho^{3+} by two cross relaxation pathways given by [73]:

$$^5F_4/\ ^5S_2\ (Ho^{3+}) + {}^2F_{5/2}\ (Ce^{3+}) \rightarrow {}^5F_5\ (Ho^{3+}) + {}^2F_{7/2}\ (Ce^{3+})$$

$$^5I_6(Ho^{3+}) + {}^2F_{5/2}\ (Ce^{3+}) \rightarrow {}^5I_7\ (Ho^{3+}) + {}^2F_{7/2}\ (Ce^{3+}).$$

Matching-energy excited states of lanthanides can couple with one another through cross relaxation multipolar interactions for doping concentration exceeding a certain threshold. Therefore, cross relaxation is a dominant radiationless relaxation at high concentration of the centers. The cross relaxation rate W_{CR} can be expressed as follows versus the concentration of the involved activators C_A $W_{CR} \cong C_M C_A{}^m$, where the excitation migration constant C_M depends on the average ion-ion spacing, m=1 for ions with fast energy diffusion and m=2 for ions with limited rate of energy diffusion [20,65,74]. Cross-relaxation is characterized by short lifetimes and decreased luminescence intensity.

3.3 Luminescence quenching

The class of luminescence quenching phenomena includes losses of radiative efficiency resulting from several contributions, such as: i) thermal quenching (non-radiative relaxation to the ground state from excited state parabolas), ii) radiationless energy transfer involving killing centers, disorder-induced states, vacancies, sensitizer or activator with changed valence, iii) absorption of the excitation energy by both luminescent centers and host lattice, iv) host absorbing the emission photon and v) concentration quenching, that is a radiationless energy transfer pathway due to concentration of the luminescent centers larger than a threshold value.

For instance, fluorescence quenching results whenever, following energy transfer from a sensitizer ion to an activator ion, the activator relaxing non-radiatively causes deactivation of the expected fluorescence and reduction of the quantum efficiency.

Energy transfer to lattice vibrations (phonons) may result in a quenching mechanisms. The rate of nonradiative energy transfer due to lattice vibration depends on the host material and the gap between energy levels in that the larger the gap, the more phonons are required to bridge the gap and the lower the probability of phonon-assisted decay is.

The most popular and critical luminescence quenching phenomenon in rare earth activated hosts is concentration quenching [75,76]. It is a known effect in Nd^{3+}-doped yttrium aluminum garnet (YAG) laser bulk crystals [77], whereby it limits the amount of the luminescent centers usable for doping. Cross relaxation can be responsible for luminescence quenching for concentration of the activator ions above a threshold value, depending on dopant and host, yielding the maximum luminescence intensity.

Theory of concentration quenching in inorganic bulk phosphors was developed on the basis of resonant transfer of electronic excitation from the absorbing center to another identical center followed by the participation of a quenching site [78]. It was found quenching of luminescence in bulk materials for concentration of the activator of 10^{-3}–10^{-2} M [78] due to energy transfer processes between dopants favored by shorter relative inter-ion distance. According to the Auzel's model, concentration quenching is active whenever the average distance between the luminescence centers is short enough to fulfill the following relationship between dopant concentration (C) and fluorescence lifetime (τ(c)) [79]:

$$\tau(c) = \frac{\tau_o}{1 - \frac{C}{c_0}\ \exp\ -\frac{N}{3}}$$

where τ_0 is the lifetime of the radiative transition, c_0 is a constant and N is the number of phonons generated via non radiative relaxation (i.e., the multi-phonon order).

High doping content favors both energy migration (i.e., transport of the excitation energy far away from the initial excited sensitizer) of excited states between neighboring sensitizers and cross relaxation between activators. In the case of center-to-center distance of a few nanometers, overlapping between

absorption and emission bands, and allowed transitions, resonant transfer by dipole-dipole mechanism can occur with high probability ($\sim 10^4$ sec^{-1}). It involves energy migration processes (energy transfer and cross relaxation) and may imply a shortening of the excited-state lifetime according to the empirical formula $\tau_{abs} = \tau_{oo}/(1+(\rho/Q)^p)$, where τ_{oo} is the lifetime in the limit of zero concentration and Q is the quenching concentration [71]. Hence, control on the doping level is critical to limit undesirable luminescence quenching. To detail, in order to obtain efficient upconversion in the hexagonal-phase alkaline rare-earth fluoride crystals, the concentration of the sensitizers and activators should be around 20 mol % and below 2 mol %, respectively. For instance, in $NaYF_4$ host lattices, the concentration of Tm^{3+} dopant should be in the range of ~0.2–0.5 mol % with ~20–40 mol% Yb^{3+} to avoid concentration quenching effects [80,81]. The threshold of concentration quenching also depends on the host crystal [79].

The occurrence of a threshold for the onset of concentration quenching is particularly critical in nanoscale luminescent materials due to the reduced volume and increasing relative fraction of dopant centers close to the surface. Turning from bulk to nanoscaled phosphors, well-designed strategies have to be applied to overcome the stringent limitations due to concentration quenching [82].

4. UPCONVERSION: fundamentals and dynamics

As overviewed, upconversion luminescence refers to emission of one photon with higher energy than the pump photon. Luminescence dynamics via upconversion in rare- earth doped phosphors can be depicted as occurring in three main stages, that is energy absorption under excitation, energy transfer and/or migration among several levels, release of energy by radiative and/or radiationless processes and emission of upconversion photons.

The basic requirement for generating upconversion luminescence is the presence of at least two metastable excited levels. Upconversion processes of singly doped phosphors are strongly affected by the distance between two neighboring activators and the absorption cross-section of dopants. The former parameter can reduce the upconversion efficiency due to cross-relaxation processes enhanced by high dopant contents that cause luminescence quenching. On the other hand, a low absorption cross-sections of the lanthanide activators negatively impacts on the pump efficiency. A strategy to increase the absorption of lanthanide-doped upconverters is the introduction of an additional dopant playing the role of sensitizer and with energy levels able to ensure efficient energy transfer to the activator dopant. In this respect, well suited lanthanide ions for upconversion are Pr^{3+}, Nd^{3+}, Ho^{3+}, Er^{3+} and Tm^{3+} that have intermediate metastable levels able to be populated by absorption of near-IR photons. Furthermore, they exhibits long-lived excited states emitting intense green and UV photons and Pr^{3+} is very versatile because it can emit blue, green and red fluorescence from the same level.

In general, photon energy, symmetry of the host materials, amount of activator and sensitizer dopants and the lattice constants play a major role in affecting the upconversion strength.

Enhanced-efficiency upconversion luminescence can be promoted by sensitizer-actuator co-doping with a sufficiently large absorption cross-section in the near-IR spectral region of the sensitizer. Since the energy level sequence of most activators is complex, phonon-related transitions are necessary to observe upconversion if the excitation light does not match the upconversion transitions. An efficient sensitizer has to have strong and broad absorption/emission to favor energy transfer to the absorption lines of the acceptor ion.

In this paragraph, the building-block mechanisms leading to upconversion luminescence are classified and discussed and, furthermore, a few examples are provided to illustrate the role played by the discrete energy levels of rare earth dopants in upconversion emission.

4.1 Mechanisms/pathways leading to upconversion emission

In general, mechanisms leading to upconversion emission can be classified into five main reference mechanisms with different efficiency: i) multi-step excited state absorption (ESA), ii) upconversion by energy transfer (ETU), iii) cooperative processes, iv) photon avalanche (PA) and v) energy migration-mediated upconversion (EMU) [20].

i) In the presence of a single kind of rare earth dopant (activator) at low concentration, the simplest example of upconversion process is two-photon excited state absorption (2-ESA, Figure 6(a)), referring to sequential absorption of two pump photons by a single ion with multiple energy levels, It can be generalized to multi-photon excited state absorption, as already discussed. In order to enable sequential absorption of several pump photons, the intermediate energy levels of the luminescent centers have to be stable and exhibit proper electron populations. In this respect, high pump power density and large absorption cross-section are favorable conditions for the occurrence of ESA processes.

While interactions between centers can be neglected at low doping concentration, under increasing dopant concentration (> 1%), centers begin to interact each other and activators may act as sensitizers, in that they transfer the excited energy to centers that assist the upconversion luminescence via intermediate processes. In this framework, non-radiative cross relaxation can deteriorate the emission intensity and, as a consequence, the probability of ESA processes decreases.

ii) Energy transfer upconversion (ETU), which is the most popular upconversion mechanism and is depicted diagrammatically in Figure 7 (a), is more efficient than ESA and is by far the most efficient upconversion mechanism in lanthanide doped upconverters. Being independent on the pump power, it results from successive energy transfer pathways between ions at different sites whenever an activator is in an excited state. In the case of activator-activator pairs (Figure 7(a), left upper panel), intermediate levels of the two centers are excited by GSA under radiative excitation followed by excitation to a higher lying energy level of one of the two centers via energy transfer. Then, while the donor ion decades to its ground state without luminescence emission, the highly excited ion decays by upconversion luminescence. Alternatively, in the presence of an activator-sensitizer pair consisting of unlike centers, only the sensitizer ion may absorb the pump photons and be excited by GSA absorption. Subsequently, the activator is excited to a higher energy level via energy transfer from the sensitizer. After that, such excited activator is promoted to a higher excited state by a second energy transfer process from the sensitizer. Finally, the activator decay via upconversion luminescence to its ground state (Figure 7(a), right upper panel). Since two energy transfer processes are involved, the above described upconversion mechanism is also termed "successive energy transfer". For instance, the ETU mechanism is the photoluminescence mechanism of Yb^{3+}-/Er^{3+}, Yb^{3+}-Tm^{3+} and Yb^{3+}-Ho^{3+} pairs. In the presence of an energy mismatch between sensitizer and activator, phonon assistance is necessary to bridge the energy gap (phonon-assisted energy transfer).

iii) Sensitization can involve one or more ions. In the latter case, the process is termed "cooperative" when active ions are distributed at sufficiently short distances they can interact each other. Figure 7(b) reports the general scheme of cooperative sensitization: the excitation energy gained by two identical ions is transferred to a third ion which is promoted to a highly excited state and, subsequently, decays via upconversion. Under this situation, if emission of one photons occurs from two excited interaction ions, then the upconversion. process is termed "cooperative luminescence" (Figure 7(c)). For instance, in purely Yb^{3+}-doped nanocrystals, the formation of Yb^{3+}–Yb^{3+} dimers can lead to blue cooperative upconversion emission [83].

In any discussed situation, pump photons have to match the energy of one transition and the upconversion emission intensity is proportional to the n^{th} power of the incident flux, where n is the number of the process's steps.

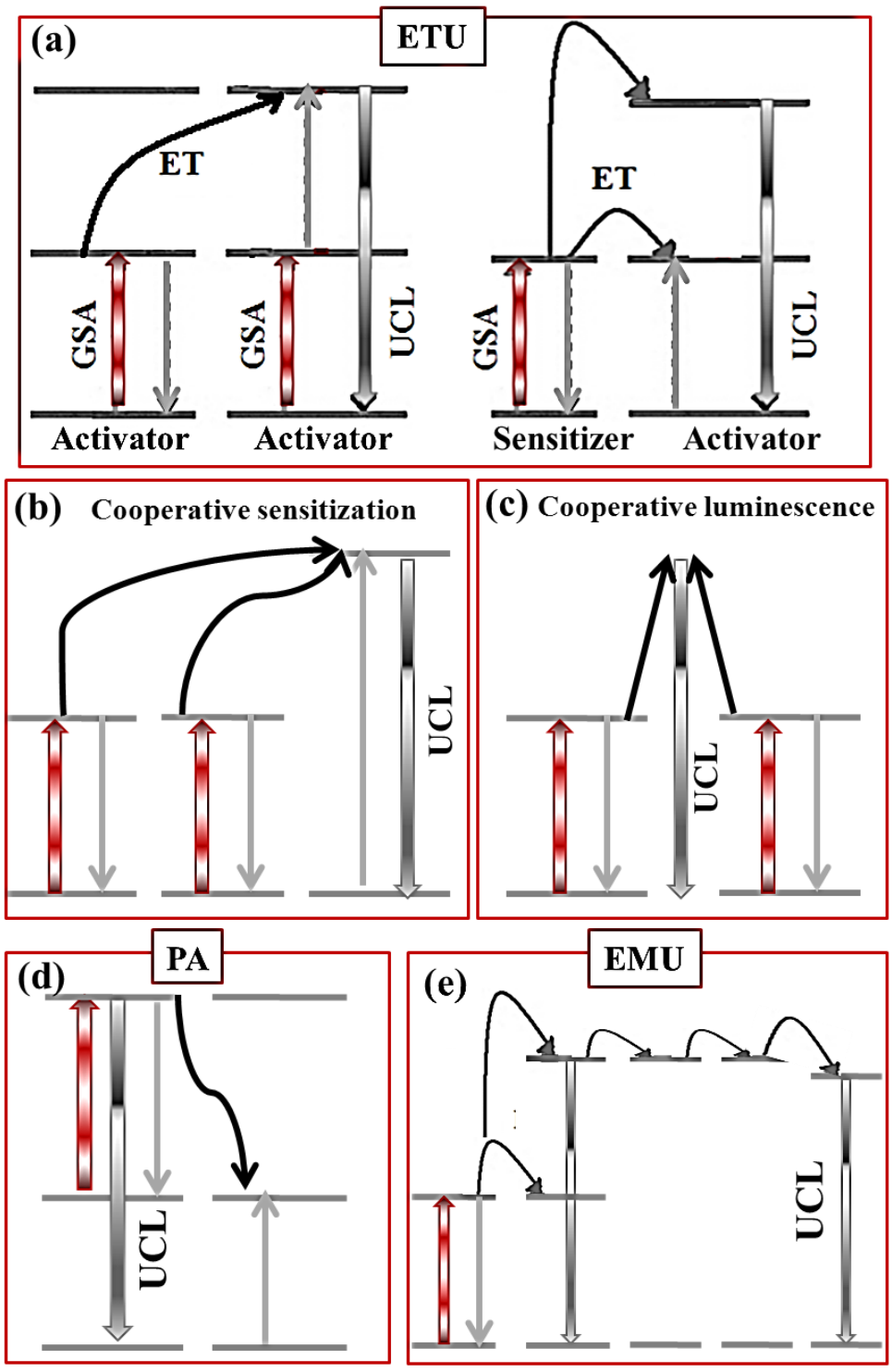

Figure 7: Schematic representations of upconversion luminescence (UCL) processes: (a) energy transfer upconversion (ETU), (b) cooperative sensitization, (c) cooperative luminescence, (d) photon avalanche (PA) and (e) energy migration-mediated upconversion (EMU). Upward red arrows refer to direct excitation processes, downward thick shadowed grey arrows refer to upconversion emission, Upward and downward light gray thin arrows indicate intermediate transitions and curved black arrows refer to energy transfer processes.

iv) Turning to the PA process [84], the simplest energy scheme of such process is represented in Figure 7(d). To detail, as the energy of the pump photon matches the energy gap between two excited states (the lower energy lying being metastable) of the upconverting ion, pumping promotes such material to a highly excited state (termed super-excited) without any resonant GSA. Subsequently, resonant cross relaxation between the super-excited level and a neighboring ground state center leads to populated intermediate states of both centers. Iteration of such mechanism enables to populate the intermediate states above the excitation threshold, hence creating favorable conditions for avalanche transitions until the depopulation of the super-excited level is less effective than that of the ground state. Upconversion luminescence following PA is poorly efficient in particular in the case of nano-upconverters [85].
v) In the absence of intermediate levels, enhanced upconversion efficiency from the activators can be obtained via the energy transfer mechanisms occurring in EMU. This process typically involves four types of luminescent ions acting as a sensitizer, an accumulator, a migrator and an activator according to the dynamics represented diagrammatically in (Figure 7(e)): an ETU process populates the higher excited state of the accumulator, the energy absorbed by the accumulator is transferred to the migrator, and sequential energy transfer between the migrator ions leads to the energy being trapped by a neighboring activator. Upconversion luminescence occurs from the activator and accumulator relaxing to the ground state. Typically, the luminescent centers yielding EMU are incorporated into separate layers (for instance, core-shell structures) with finely tuned concentrations.
In general, relaxation rates, energy transfer probability, rare earth concentration and energy mismatch (meaning eventual participation of phonons) play a role in the efficiency of the process that is determined by the efficiency of the several stages of the whole upconversion process [20].

4.2:Examples

In the case of singly doped upconverting phosphors, the most widely used activators are Er^{3+}, Tm^{3+}, and Ho^{3+} owing to their energy levels well matching the energy of the most commonly exploited transition ($^2F_{7/2} \rightarrow {}^2F_{5/2}$) of Yb^{3+} ion under 980 nm excitation.

4.2.1. Single doping: Er^{3+} ion

Figure 8(a) shows a schematic diagram of the energy level structure and transitions (both radiative and phonon-mediated) of trivalent Er^{3+} excited via photon absorption at 980 nm. Noteworthy, several pairs of energy levels (for instance $^4I_{11/2}$ -$^4I_{15/2}$ and $^4I_{11/2}$-$^4F_{7/2}$) are separated by an energy gap of 1.27 eV (corresponding to the wavelength value of 980 nm). This fact can be exploited to induce efficient upconversion luminescence under excitation at 980 nm of Er^{3+} ions. The radiative emission transitions of Er^{3+} are listed in Table 1 (left column) and typical upconversion processes of $Er^{3+}$are depicted in Figure 8(b). The emission spectrum of Er^{3+} is usually dominated by the $^4S_{3/2} \rightarrow {}^{4I}1_{5/2}$ transition (~660 nm) and $^4F_{9/2} \rightarrow {}^4I_{15/2}$ transition (~540 nm) in α-$NaYF_4$ and β-$NaYF_4$, respectively, host crystals with emission efficiency higher in β-$NaYF_4$ than in α-$NaYF_4$ [86]
Operatively, upon excitation at 980 nm, rather than being excited to the $^4F_{7/2}$ level, Er^{3+} ions in the $^4I_{11/2}$ level can decay to the $^4I_{13/2}$ level, followed by excitation to the $^4F_{9/2}$ level via phonon assisted energy transfer. As a result, Er^{3+} ions can relax radiatively by at least three different transitions, that is green emission (525/545 nm by the $^2H_{11/2} \rightarrow {}^4I_{15/2}$ and $^4S_{3/2} \rightarrow {}^4I_{15/2}$ transitions) and red emission (656 nm by the $^4F_{9/2} \rightarrow {}^4I_{15/2}$ following two-step photon absorption). The 4 $I_{13/2}$ level of Er^{3+} is metastable.
Turning to a co-doping example, the hexagonal NaYF4 fluoride crystal (β-$NaYF_4$ phase) co-doped with Yb^{3+}-Er^{3+} or Yb^{3+}-Tm^{3+} pairs is one of the most efficient up-converter under excitation at 980 nm [86]. In $NaYF_4$, the Yb^{3+} and Er^{3+} dopants substitute the host Y^{3+} ions without changing the crystal structure.

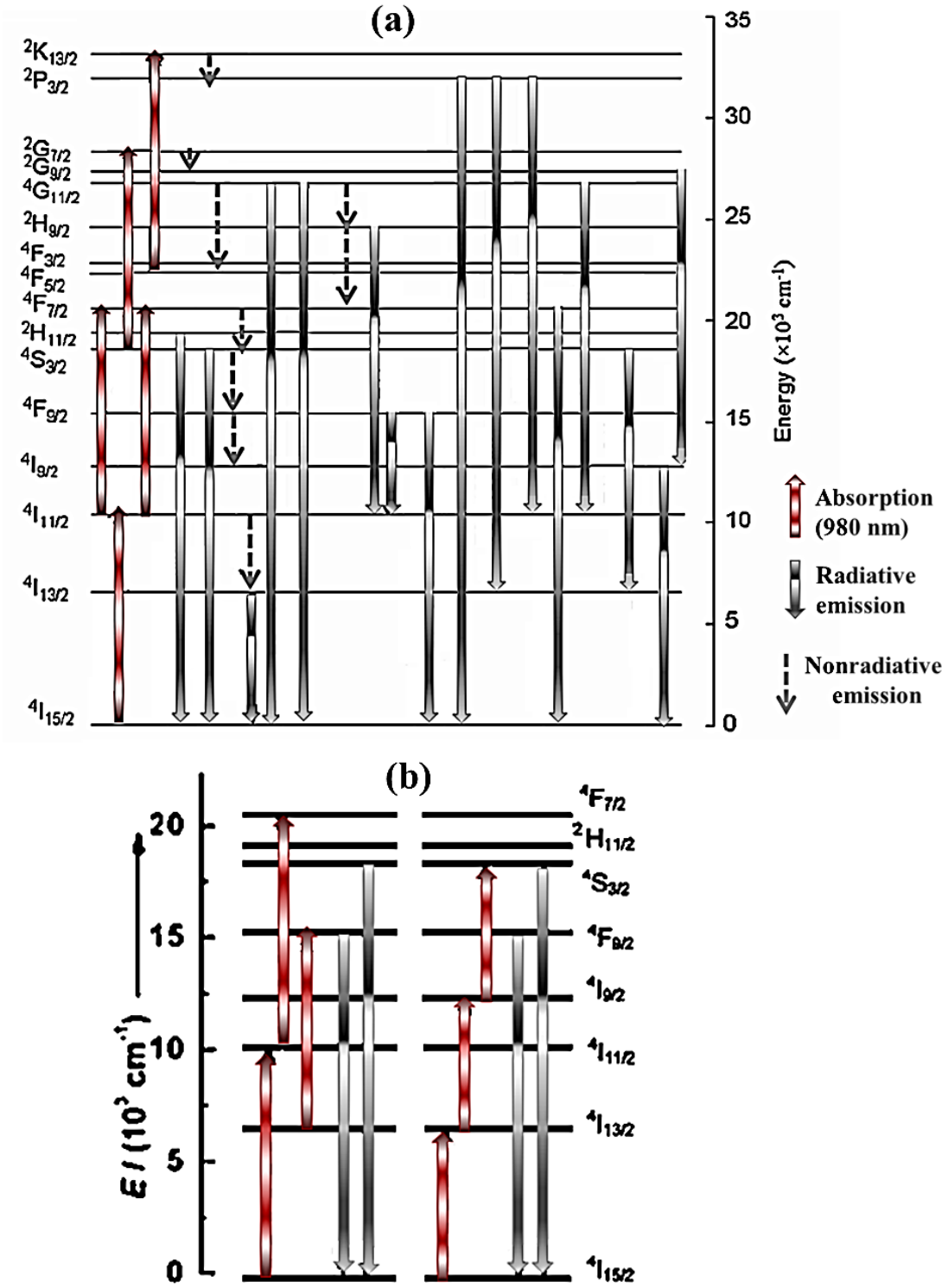

Figure 8 Schematic diagram of **(a)** the energy level structure and radiative (straight arrow) as well as nonradiative decay transitions of Er^{3+} and (b) typical upconversion processes of Er^{3+}

Table 1: Radiative emission transitions of Er^{3+}, Tb^{3+}, Nd^{3+} and Tm^{3+} lanthanide ions, where fluorides are suitable hosts for upconversion. The upconversion transitions are labeled by the acronym UC.

Er^{3+}		Tb^{3+}		Nd^{3+}		Tm^{3+}	
Transition	**λ (nm)**	**Transition**	**λ (nm)**	**Transition**	**λ (nm)**	**Transition**	**λ (nm)**
$^2P_{3/2} \rightarrow {}^4I_{15/2}$	320	$^5D_3 \rightarrow {}^7F_6$ (UC)	381	$^2P_{1/2} \rightarrow {}^4I_{9/2}$	430,	$^1I_6 \rightarrow {}^3F_4$	290
$^4G_{11/2} \rightarrow {}^4I_{15/2}$	383	$^5D_3 \rightarrow {}^7F_5$ (UC)	415	$^2P_{1/2} \rightarrow {}^4I1_{1/2}$ (UC)	482	$^1I_6 \rightarrow {}^3F_4$	345
$^2P_{3/2} \rightarrow {}^4I_{13/2}$	403	$^5D_3 \rightarrow {}^7F_4$ (UC)	438	$^2P_{1/2} \rightarrow - {}^4I_{13/2}$(UC)	525	$^1D_2 \rightarrow {}^3H_6$	362
$^2H_{9/2} \rightarrow {}^4I_{15/2}$ (UC)	415	$^5D_4 \rightarrow {}^7F_6$ (UC)	489	$^4G_{7/2} \rightarrow - {}^4I_{9/2}$, (UC)	535	$^1D_2 \rightarrow {}^3F_4$	450
$^2P_{3/2} \rightarrow {}^4I_{11/2}$	470	$^5D_4 \rightarrow {}^7F_5$ (UC)	541	$^2P_{1/2} \rightarrow - 4I_{15/2}$, (UC)	580	$^1G_4 \rightarrow {}^3H_6$	475
$^2H_{11/2} \rightarrow {}^4I_{15/2}$ (UC)	525	$^5D_4 \rightarrow {}^7F_4$ (UC)	584	$^4G_{7/2} \rightarrow - {}^4I_{11/2}$ $^4G_{5/2} + {}^2G_{7/2} \rightarrow - {}^4I_{9/2}$(UC)	600	$^1G_4 \rightarrow {}^3F_4$	644
$^4S_{3/2} \rightarrow {}^4I_{15/2}$ (UC)	542	$^5D_4 \rightarrow {}^7F_3$ (UC)	619	$^4G_{7/2} \rightarrow - {}^4I_{13/2}$(UC)	664	$^3F_3 \rightarrow {}^3H_6$	694
$^4S_{3/2} \rightarrow {}^4I_{15/2}$ (UC)	550			$^4G_{7/2} \rightarrow - {}^4I_{15/2}$ (UC)	766	$^3H_4 \rightarrow {}^3H_6$	803-825
$^4G_{11/2} \rightarrow {}^4I_{11/2}$	618					$^1D_2 \rightarrow {}^1G_4$	1510
$^4F_{9/2} \rightarrow {}^4I_{15/2}$ (UC)	656						
$^4G_{9/2} \rightarrow {}^4I_{9/2}$	667						
$^4I_{9/2} \rightarrow {}^4I_{15/2}$	793						
$^4S_{3/2} \rightarrow {}^4I_{13/2}$	849						
$^4I_{13/2} \rightarrow {}^4I_{15/2}$	1540						

4.2.2. Co-doping: Yb^{3+}-Er^{3+} and Yb^{3+}-Tm^{3+} pairs

An excellent sensitizer for photon upconversion isYb^{3+} due to its high absorption cross-section ($9.11 * 10^{-21}$ cm^{-2}) at 976 nm ($^2F_{7/2} \rightarrow {}^2F_{5/2}$ transition) among lanthanides and very simple energy diagram including one excited state (the level $^2F_{5/2}$) close in energy to levels of Er^{3+} and Tm^{3+} (Figure 9). Hence the Er^{3+}-Yb^{3+} pair is an optimal activator- sensitizer pair for upconversion luminescence under excitation at the 980 nm laser-diode wavelength [87]. On the other hand, closely spaced energy levels of an activator can have a negative impact because the rate of non-radiative relaxations decreases exponentially with increasing separation between its levels. On this basis, $Er^{3+}$and Tm^{3+} are ideal ETU activators [88,89].

In this framework, efficient multicolor upconversion luminescence was demonstrated in colloidal lanthanide $NaYF_4$ nanoparticles codoped with Yb^{3+}-Er^{3+} and Yb^{3+}-Tm^{3+} pairs, leading to strong yellow and blue emissions [90]. The efficent infrared-to-visible upconversion allowed by the Yb^{3+}-Er^{3+}system works according to the mechanism indicated schematically in Figure 9(a). Yb^{3+}ions have a simple structure of electronic levels and energy matching between the transition $^2F_{7/2} \rightarrow {}^2F_{5/2}$ and the exciting wavelength 980 nm of laser diodes. Moreover, the excited states of Yb^{3+} ions also match with excited levels of Er^{3+}, Tm^{3+}, and Ho^{3+}, hence enabling energy transfer processes. In the case of the Yb^{3+}-Er^{3+} pair, an Yb^{3+} ion excited into the $^2F_{5/2}$ level via $^2F_{7/2}$ - $^2F_{5/2}$ upward transitions relaxes by raising an Er^{3+} ion to the $^4I_{11/2}$ level (transition $^4I_{15/2}$-$^4I_{11/2}$). Subsequently, another Yb^{3+} ion excited into the $^2F_{5/2}$ level relaxes and promotes the previously excited Er^{3+} to the higher energy $^4F_{7/2}$ level. Phonon-induced relaxation occurs between the small energy gap levels lying above the $^4S_{3/2}$ state and, finally, green emission at 540 nm via the transition $^4S_{3/2} \rightarrow {}^4I_{15/2}$ and red emission via the transition $^4F_{9/2} \rightarrow {}^4I_{15/2}$ yield upconversion luminescence. Fast resonant energy transfer of the excitation among Yb^{3+} ions boosting the upconversion emission requires relatively high (10% or greater) concentration of Yb^{3+}.

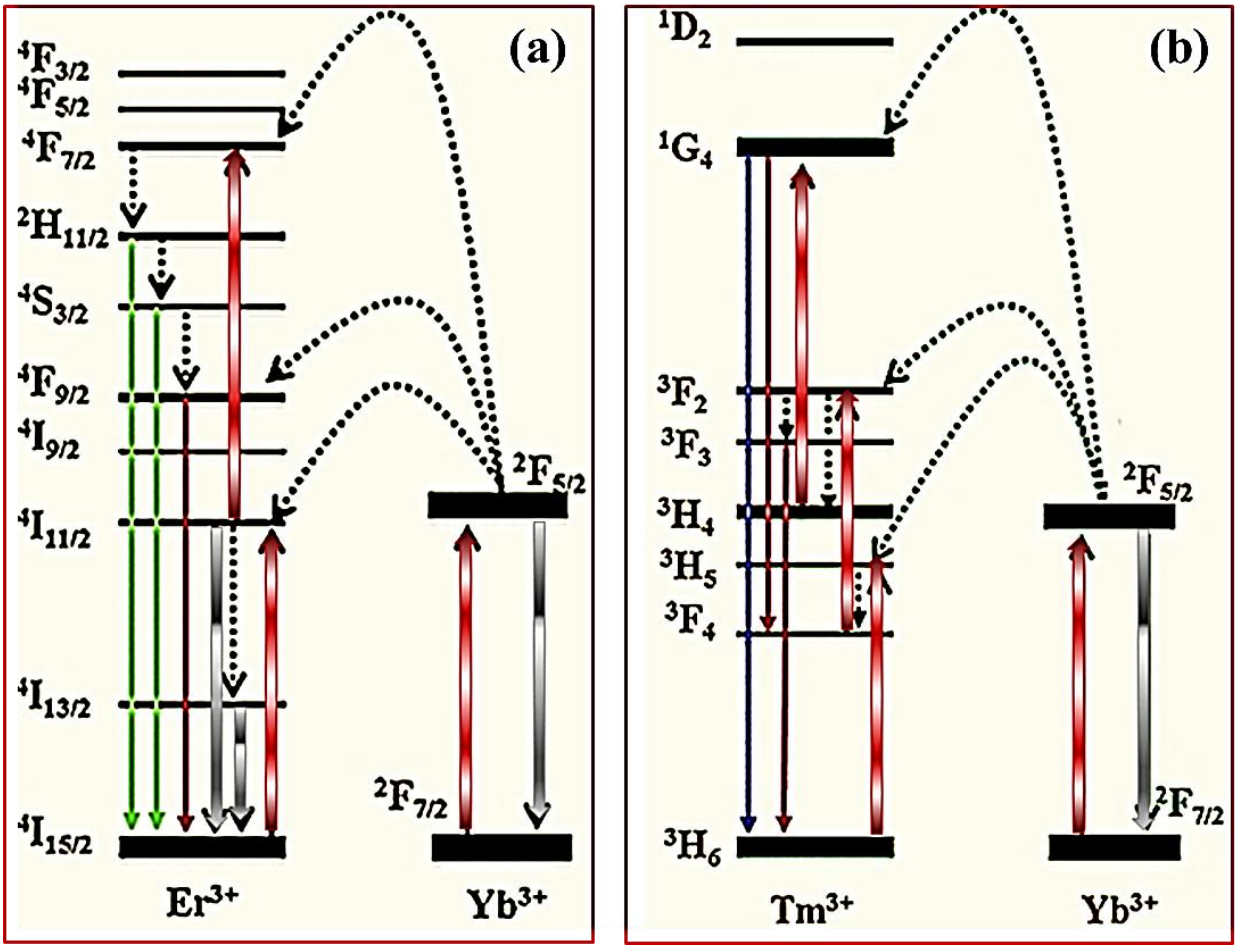

Figure 9 Scheme of the energy levels of Yb3+, Er3+ and Tm3+ ions pointing out the energy transfer mechanisms concurring to the upconversion luminescence resulting by Yb^{3+}–Er^{3+} and Yb^{3+}–Tm^{3+} pairs under excitation at 980 nm,

Analogous dynamics occurs in the case of Tm^{3+}-Yb^{3+} pairs (Figure 9(b)) that, under excitation at 980 nm, yield UV emissions at 290 nm (five-photon process), 345 nm (five-photon process) and 362 nm (four-photon process), visible emissions at 450 nm (four-photon process), 475 nm (three-photon process), 644 nm (three-photon process) and 694 nm (two-photon process), and near-IR emission at 800 nm (two-photon process) (Table 1). Cross-relaxation plays a role in Er^{3+}-Tm^{3+}co-doped upconverters through the $^2I_{11/2}$ + $^2H_{11/2}$-$^4I_{13/2}$ + $^4F_{3/2}$ and $^4F_{7/2}$ + $^2H_{11/2}$-$^2H_{9/2}$($^2G_{9/2}$) + $^4F_{9/2}$ channels that weaken the green emission from the $^2H_{11/2}$, $^4S_{3/2} \rightarrow {}^4I_{15/2}$ transitions and enhance the red emission from $^4F_{9/2}$ as well as the blue emission from $^2H_{9/2}$ [20,72] .

By comparison with the Yb^{3+}–Er^{3+} pair , the discrete and ladder-like, rather than dense, distribution of the energy levels of Tm^{3+} implies that more than two-photons can be involved in the upconversion emission from the Yb^{3+}–Tm^{3+} coupling as well as reduced probability of multi-photon upward transitions. Under the application of the 980 nm excitation wavelength, the excited electrons relax to the ground state $^4F_{7/2}$ of Yb^{3+} and a radiationless energy transfer process occurs to the $^3H_5$ state of a Tm^{3+} followed by electron relaxing to the $3F_4$ state that allows the $^3F_4 \rightarrow {}^3F_2$ upward transition via resonant energy transfer from Yb^{3+}. Then, relaxation processes populate the $^3F_3$ and $^3H_4$ states and $^3F_3$ - $^3H_6$ (694 nm) and $^3H_4$ - $^3H_6$ (800 nm) transitions are induced. For increasing pump power, the $^3H_4$

$\rightarrow {}^1G_4$, ${}^1G_4$-${}^1D_2$ and ${}^1D_2$-${}^3P_2$ upward transitions can be prompted that result in the ${}^1G_4 \rightarrow {}^3F_4$ (644 nm), ${}^1G_4 \rightarrow {}^3H_6$ (475 nm), ${}^1D_2 \rightarrow {}^3F_4$ (450 nm), ${}^1D_2 \rightarrow {}^3H_6$ (362 nm), ${}^1I_6 \rightarrow {}^3F_4$ (345 nm) and ${}^1I_6 \rightarrow {}^3H_6$ (290 nm) radiative decay transitions. The concentration of Yb^{3+} dopant is usually kept at 20% or higher in combination with much lower (less than 2%) content of the activator to minimize undesirable multi-photon cross-relaxations favored by complex and dense energy level structure of the activator.
Noteworthy, the presence of radiationless relaxations, competition between several energy transfer pathways, upconversion and down conversion transitions as possible sources of energy losses. For instance, generation of white light emission via upconversion in triply doped (usually Tm^{3+}, Er^{3+},or Yb^{3+}, for absorption of Yb^{3+} and energy transfer from Yb^{3+} to Er^{3+}/Tm^{3+} ions) oxide and fluoride hosts to overlap sharp red/green/blue emission lines suffers from energy quenched by means of unexpected cross relaxation processes.

5. Nano- upconverters

5.1 Introduction and relevant applications

Similarly to bulk inorganic phosphors, commonly, nano-sized inorganic phosphors exhibiting upconversion (referred to as "nano-upconverters" hereafter) consist of a nominally pure host crystal doped with a proper kind, combination and amount of activator and/or sensitizer centers characterized by multiple energy levels. In this scheme, a sensitizer with high cross section areas absorbs the pump photons efficiently and transfers the gained excitation energy to the activator, having ladder-like multiple intermediate excited states, via several intermediate energy transfer pathways. An excited state of the activator matching the energy provided by the sensitizer and with long enough lifetime (i.e., a few microsecond) is needed to yield visible and even ultraviolet upconversion emission from the high energy levels of the activator [91]. A typical example of nano-upconverter is $NaYF_4$ nanocrystalline system doped with Yb^{3+} ions acting as sensitizers and Tm^{3+} or Er^{3+} ions working as activators (emitters).
Although the composition of nano-upconverters mimics bulk phosphors, important and peculiar differences stem from the spatial confinement that will be overviewed in the following discussion and examples.
As a first remark, size-confinement effects playing a role in the field of nanophosphors should not be confused with quantum size effects (i.e., quantum energy spectrum and blue-shift of the band-gap for decreasing size) that determine the spectral response of semiconductor quantum dots [92]. Although several kinds of luminescent nano-sized upconverters have been reported in the literature (eg, graphene quantum dots, CdSe and CdS nanoparticles, CdSe/InP colloidal nanoparticles, PbSe/CdSe/CdS heterostructures [93-96], rare-earth doped nano-upconverters exhibit several peculiarities. For instance, the emission spectrum of semiconductor quantum dots is strongly dependent on the nanoparticle size (quantum size effects) and, due to blue-shift of the energy band gap for decreasing size, excitation may require UV pump photons. Such effects are not active in rare-earth activated nanophosphors [35], where scaling down the size to the nanoscale makes critical the role played by the surface-to-volume ratio, surface-related defects and disordering, dopant site symmetry, phase of the crystalline matrix, dopant-ligand distance and strength of the coordination, distribution of activator-sensitizer ions, surface composition and coordination [97]. On the other hand, nano-upconvertes do not exhibit host-sensitized emission due to lanthanides dopants, meaning that lanthanide dopants play a key role in each step of the processes leading to upconversion luminescence. Moreover the 4f electrons of rare earth ions being shielded by the outer 5s and 5p electrons, their electronic transitions involving the f levels present long lifetime emission and narrower bandwidth than quantum dots [88,98-100] as well as a larger number of discrete energy levels with multiband emission ranging from the visible to the short wavelength IR radiation. Further, rare-earth doped upconverters can be photo-excited by near-IR low-energy photons

in the optimum transparency window of the biological tissues, that involves deeper penetration depth in biological tissues, noninvasive photo-treatment and reduced damaging to biological samples due to avoided UV excitation. In this respect, limitations (for instance, high signal-to-noise ratio and limited sensitivity) of the most fluorescent down-converting materials (dye molecules, quantum dots, and dye-doped silica/gold nanomaterials) in terms of their excitation sources (ultraviolet (UV) or visible light) inducing photo-damage to biological specimens and autofluorescence has prompted the applicative interest in nano-upconverters [101]. Additionally, the metastable energy levels of the trivalent lanthanide ions are favorable to the establishment of population inversion and amplified stimulated emission at relatively low pump power. From the applicative standpoint, excitation in the optical window allowed by upconversion open the way to applicative opportunities of nano-upconvertes as luminescent markers in the diagnosis and therapy field of luminescence biomedical imaging and labeling with negligible auto-fluorescence of the biological background [102,103]. As a further remark, the advantage of efficient multi-photon energy transfer makes single nano-upconverters detectable under conditions of low excitation power density (~ a few hundred W/cm^2) suitable for in vitro and in vivo bio-imaging [104,105], near-infrared induced photothermal therapies [106] single particle tracking [107], deep tissue nano-thermometry sensing [108]. Hence, rare earth-activated nano-upconverters represent a valid alternative to organic fluorophores and quantum dots due to large anti-Stokes shifts (up to 500 nm), long luminescence lifetime (metastable energy levels), excellent photo-stability, high color purity, high quantum yields, quantum cutting, weaker auto-fluorescence background under IR excitation, deep penetration lengths of IR radiation in biological specimens and tissue, minimum background noise in the case of applications in vivo, low cytotoxicity to a broad range of cell lines, absence of photo-blinking and photo-bleaching [37,100,109-113]. The many advantageous properties of nano-upconverters have favored a broad range of applications, including, in addition to the above mentioned, lighting [45,114,115], displays [39,116], optical imaging [117,118] , drug delivery [109,119], bio-imaging and biomedical imaging [106,120-122], magnetic resonance tomography [123], photovoltaic devices [124], lifetime multiplexing [125], photochemical reactions [126], biosensing, super-resolution microscopy and nanoscopy [127], nano-thermometry in cells [128], short wavelength IR radiation imaging [118], photodynamic therapy [129], labelling for in vitro and in vivo photoluminescence bioimaging [104,130], bioassays [131,132], amplified stimulated emission [72].

5.2 Spatial-confinement –related phenomena/effects

New pathways in the research field of nano-phosphors date to the first observation of two peculiar aspects occurring in Mn^{2+}-doped ZnS nanocrystals [133]. First, room-temperature photoluminescence quantum efficiency was found to increase with decreasing size R (from < 1% at R=70 Å to nearly 18% at R=3.5 Å) leading to efficiency comparable to the bulk material. This finding was tentatively associated with chemical passivation of the surface of the nanocrystalline powders and reduction of surface-related radiationless recombinations due to the introduction of the Mn impurity. Second, by comparison with the bulk counterpart, experimental evidence demonstrated luminescence lifetime of the Mn^{2+} $^4T_1 \rightarrow {}^6A_1$ transition faster by more than 5 orders of magnitude (ns versus ms) in the presence of high radiative efficiency (~ 20%). This effect was interpreted as a result of the confinement-related enhanced importance of the nanocrystal surface leading to faster trapping and recombination times in the energy transfer between the host crystal and the Mn dopant due to increased overlap (mixing) of the s-p and d-f wave functions of host and Mn dopant, respectively. In the case of ZnS nanoparticles doped with Mn^{2+}ions, although efficient upconversion results from two-photon excitation [134], broadband emission from the d – d transition in Mn^{2+} is not suitable for biological labeling and imaging applications. Hence, in the perspective to exploit sharp emission lines, rare earth dopants were considered as a suitable alternative. Strong upconversion luminescence of both dopants was reported in Mn^{2+}-Eu^{3+} co-doped ZnS nanoparticles [135].

Nanoscale-induced emission enhancement and tunability were also reported in the case of yttrium oxide (Y_2O_3) nanoparticles co-doped with Yb^{3+} and Er^{3+} ions [136] and for decreasing particle size (from 55 to 13 nm) due to the small exciton Bohr radius [87].

Efficient multicolor upconversion emission in $NaYF_4$ nanocrystals was first demonstrated in the presence of Er^{3+}-Yb^{3+} and Yb^{3+}-Tm^{3+} pairs [90,137]. Noteworthy, $NaYF_4$ nanocrystals have been intensely investigated as highly efficient upconversion host materials [86] enabling a so high brightness that single upconverting nanocrystals as small as 27 nm can be observed in confocal microscopy analysis [138] .

In the case of Er^{3+}-Yb^{3+} co-doped $NaYF_4$ nanocrystals, increased red-to-green intensity ratio and reduced luminescence lifetimes were observed for decreasing size [139]. As already described, under 980 nm laser excitation of Er^{3+}-Yb^{3+} co-doped $NaYF_4$ nanocrystals, Yb^{3+} sensitizers absorb the pump photons via the $^2F_{7/2} \rightarrow {}^2F_{5/2}$ transition and the nearby Er^{3+} ions are promoted to the $^4F_{7/2}$ excited state by a two-step energy transfer from the excited Yb^{3+} centers. Then through increasing population of the radiatively emitting states of Er^{3+} ions via phonon-assisted processes, Er^{3+} ions emit in the green ($^2H_{11/2}$, $^4S_{3/2} \rightarrow 4I_{15/2}$ transitions) and red ($^4F_{9/2} \rightarrow {}^4I_{15/2}$ transition) spectral range by upconversion [20,90]. Because of energy transfer losses due to the non-radiative decays $^4I_{11/2}/{}^4I_{13/2}$ (3598 cm^{-1}) and $^4S_{3/2}/{}^4F_{9/2}$ (3142 cm^{-1}) playing a major role for decreasing size, the competition between red and green emissions results in a relatively higher red-to-green emission ratio in nanocrystals. In addition to size-dependence of the green to red emission ratio at constant incident power [139], such quantity depends on the excitation power too. In regard to the influence of the excitation density, the relationship $I = P^n$, where P is the excitation density, I is the upconversion emission intensity and n is the number of near infrared excitation photons required to emit one upconversion photon, is valid under the assumption of a low density excitation [5].

The spatial confinement may add complexity in the energy migration and transfer processes, as the case of Er^{3+} ion demonstrates: under the excitation of 980 nm, combination of several mechanisms (cross relaxation and/or saturation effect of intermediate emitting levels) is responsible of different n values for the two emissions at 545 nm and 650 nm that would require a two-photon process, based on the energy matching principle. In this respect, the upconversion intensity of both green and red outputs was found to change according to the law P^n, where n is a power ranging between 1 and 2 and P is the excitation power [139] due to the relevant contribution of cooperative upconversion and negligible emission from intermediate states [140]. The key quantity is the power density of the excitation-light that may affect the entire process leading to upconversion emission through the initial deployment of the excited states. Since under high density excitation more sensitizer ions (Yb^{3+} ions) are in the excited state, during the sensitizer-to-activator energy transfer saturation may occur if the number of activators is not large enough. Hence, high density excitation would require increasing doping level of the activator ions [141]. For instance, the quenching concentration of Tm^{3+} ions was reported to be 0.2–0.5% under low excitation conditions (below 100 W cm^{-2}) and to increase up to 8% under excitation power density of 2.5 x10^6 W cm^{-2}. Similarly, for Er^{3+} –doped β-$NaYF_4$ nano-upconverters [142]: whereas the brightness is higher with 20% Yb^{3+} and 2% Er^{3+} than with 20% Yb^{3+}, 25% Gd^{3+} and 20% Er^{3+} under excitation power-density of 3x10^4 W cm^{-2}, the Er^{3+} enriched nanoparticles over-perform the conventional counterpart when the power density is increased above 3x 10^6 W cm^{-2}.

On the other hand, in Er^{3+}-Yb^{3+} codoped $NaYF_4$ nanocrystals, due to $Er^{3+} \rightarrow Yb^{3+}$ back-energy transfer induced by large content of Yb (25-60 mol%), decreased population of the excited levels of Er^{3+} ($^2H_{9/2}$, $^2H_{11/2}$, $^4S_{3/2}$) yields decreased blue and green outputs and, consequently, luminescence tunable from yellow to red [143]. Hence, deliberate and proper control on the doping concentration enables to tune the emission colors across a wide spectral range based on balanced overlapping of several emission bands and tuning of their intensity ratio. The same effect can be achieved by exploiting the lattice

structure. Indeed, more effective dopant-related symmetry breaking in the host material can result from site distortion and surface lowered coordination favored by size reduction below 100 nm. From the spectroscopy point of view, rare earth dopant-ligand distance and site symmetry affected by the spatial confinement may induce changes in the J-L coupling and J mixing effects of the rare earth states with respect to the lower energy levels [23]. This aspect points out how rare earth emission is not completely independent on the host material, which may affect the spectroscopic response of lanthanide dopants by lattice vibrations and crystal field site symmetry [144] as well as ion-ligand bonding length if multiple lattice sites occur [29,145]. An applicative issue that can clearly explain this important point is multicolor tuning under excitation by a single wavelength source. For instance, Dy^{3+}-ions present two main emission bands: the characteristic blue luminescence (470-500 nm, $^4F_{9/2} \rightarrow {}^6H_{13/2}$ transition given by a single decay component between Dy^{3+} ions) and a yellow emission (560-600 nm, $^4F_{9/2} \rightarrow {}^6H_{15/2}$ transition) very sensitive to the host material. Hence, a proper content of Dy^{3+} ions occupying not equivalent lattice sites in oxides results in changes of the yellow-to-blue intensity ratio versus Dy^{3+} -ligand bonding length [146,147].

Therefore, in lanthanide-doped nano-upconverters, artificial control on the doping content (i.e., dopant-to-dopant spacing) lets cover the entire visible spectrum color output by modulation of the intensity ratio between different emission bands related to the involved lanthanide dopants [143]. Remarkably, lanthanide assisted energy transfer and poor sensitivity of the lanthanide's orbitals to its surroundings imply that inter-dopant energy transfer pathways may be modulated by the dopant-to-dopant coordination changed by miniaturization and dopant-to-dopant distance changed by doping concentration.

Another interesting aspect is the size-dependence of the crystalline phase because the upconversion luminescence efficiency can depend on the phase of the host. For instance, in $NaYF_4$ bulk crystal and large-size nanocrystals, the upconversion efficiency was reported to be one order of magnitude larger in the hexagonal β-phase than in the cubic α-phase [31,39,148]. Interestingly, the opposite effect was observed in nanocrystals smaller than 40 nm: for size in the range 10-25 nm, the emission is stronger in α-phased $NaYF_4$ than in β-phased $NaYF_4$ nanoparticles [39]. Noteworthy, $NaYF_4$ nanocrystals were observed to turn from the β-phase to the α-phase for decreasing size from 20-45 nm to 6-14 nm [139].

A novel approach to increase the radiative transition rates in Yb^{3+}-Er^{3+} codoped nano-upconverters based on local symmetry distortion was recently reported [149]: Y ions were progressively removed from the β-phase of $NaYF_4$ nanocrystals and replaced by a 1:1 mixture of Gd^{3+} and Lu^{3+} that expand and contract the lattice, respectively. The obtained In β-$NaY_{0.8-2x}Gd_xLu_xF_4$: $Yb_{0.18}Er_{0.02}$ sub-25 nm unshelled nanocrystals, for x varied from x = 0 to x = 0.24, showed a maximum quantum yield value of 0.074% under excitation at 63 W/cm^2 of power density

5.3 Quenching effects

In addition to observable effects on output color modulation and upconversion efficiency of nanocrystals, the doping content, that determines the inter-dopant spacing, may also impact on the radiative processes resulting from interaction between lanthanide dopants due to an inherent upper limit to the dopant content at the nanoscale and the role played by the surfaces yielding quenching effects.

For example, upon decreasing the size of the nanoparticle, several effect occurs: first, the hopping length and the probability of donor-to-acceptor energy transfer are lowered due to decreasing probability that a donor can find a neighboring matching acceptor; second, the numbers of acceptors and donors decrease; and third, defect sites can prevent efficient energy migration by trapping effects.

As a significant fraction of surface atoms, enriched surface defects and organic ligands acting as quenchers affect the photophysical behavior of lanthanide-doped nano-upconverters, luminescence yield may be reduced with respect to the efficiency of the bulk counterparts. For increasing surface area fraction, high-doping concentration may cause both cross-relaxation and energy migration to the

surface quenchers due to shorter distance between dopants enhancing the probability of energy transfer pathways [150,151].

Therefore, in nanoparticles increasing the sensitizer and/or activator content may drive the system from a situation of enhanced emission brightness (due to increasing number of active centers with decreasing spacing) to a situation whereby both energy transfer within the excited levels of the sensitizer-sensitizer network and inter-activator cross relaxation as well as non-radiative energy migration decrease the luminescence efficiency [82].

In general, increasing the content of the sensitizer ions may favor either the absorption of the pump energy or energy migration between the sensitizer ions and, additionally, activator to sensitizer back energy transfer pathways. On the other hand, increasing the content of the activator ions may promote harmful cross relaxation processes and, as a consequence, concentration quenching effects [136]. Although concentration quenching also manifests at the nanoscale, the concentration threshold of dopants for observing suppressed luminescence is advantageously higher in nanophosphors than in bulk phosphor [152]. For instance, under increasing content of Tb^{3+}dopant in Y_2O_3 nanoparticles, it was observed concentration quenching at doping level above 5% in large sized particles and enhanced luminescence intensity at dopant amount of 50% in as small as 3 nm nanoparticles [153]. As a further example, for increasing excitation irradiance from 1.6×10^4 to 2.5×10^6 Wcm−2, luminescence intensity was found to increase a factor of 5.6, 71 and 1105 for Tm^{3+} content of 0.5, 4 and 8%, respectively [152]. Analogously, in Er^{3+}- Yb^{3+} co-doped sub-10 nm $NaYF_4$ nanoparticles, 20% Er^{3+} enables much higher brightness than 2% Er^{3+} under increasing excitation power [142]. A similar trend was reported in Y_2O_3 nanoparticles doped with Tb^{3+} that exhibit concentration quenching at dopant content above ~5% in large sized particles and increasing luminescence intensity at dopant amount of 50% in ultra-small (3 nm) particles [153]. Such experimental evidence was ascribed to reduced probability of ion-ion energy transfer because of out of resonance conditions and no participation of phonon modes in energy transfer [154].

Turning from bulk to nanoscale-sized materials, whenever phonon is involved through multiphonon recombination and phonon-assisted energy transfer, spatial confinement impacts on energy transfer in nano-phosphors in that the energy transfer rate decreases due to changes in the phonon density of states and limits in the number of activator-sensitizer pairs [59,154]. As it will be detailed later, the discrete character of the phonon density of states in nanocrystals relaxes the selection rules, decreases the overall electron-phonon coupling strength with increasing size, removes many low frequency phonon states [154-157].

The above discussion points out a main difference between bulk and nano-phophors: the upconversion luminescence efficiency of nano-scaled materials is inherently lower than the bulk counterparts due the presence of surface-bound activators and defects (traps, solvent molecules, oxygen, etc) acting as luminescence quenchers and perturbing energy transfer pathways [158]. Basically, in nanocrystals energy transfer can involve ion-ion, ion-defect, ion-ligand and particle-particle pairs. In general, high upconversion efficiency requires co-doping whereby sensitizer ions alongside activator ions have a closely matched intermediate-excited state [151].. As the relatively low doping concentrations of the sensitizer and activator dopant ions impacts on the brightness and upconversion efficiency of nano-upconverters, a straightforward way to improve their upconversion performance would be to increase the concentration of the sensitizer and activator species. Such strategy, however, may result in limiting concentration quenching effects [82,159]. Indeed, in nanomaterials a relevant decrease in luminescence intensity is related to three main effects: first, dopant concentration is limited by the spatial confinement; second, a large number of surface quenchers (such as lattice defects and solvent molecules) is favored by decreasing size, and, third, increasing doping level facilitates both the energy migration from the (mainly sensitizer) excited levels to the surface quencher states and the inter-activator cross-relaxation [151,159,160].

For example, typically, in order to obtain upconversion emission, Yb^{3+} ions act as sensitizer ions to transfer energy to the activator ions (Er^{3+}, Tm^{3+} or Ho^{3+}) [20]. In the case of near-IR upconversion emission of Tm^{3+} at 808 nm, the simple energy scheme of Yb^{3+} enables to increase remarkably the content of Yb^{3+} (for instance from 20 to 98%) without promoting concentration quenching because Yb^{3+} has only one excited state matching the excitation energy and being different as compared to Tm^{3+} [161]. For comparison, the doping concentration of lanthanide dopants is usually almost low, that is in the range of 0.2-2% for activators (Er^{3+}, Tm^{3+}, Ho^{3+}) and of 20-40% for sensitizers (Yb^{3+}).
In the case of the Nd^{3+}-Yb^{3+} co-dopant pair, Nd^{3+} ions absorb photons at around 800 nm and Yb^{3+} ions enable the energy transfer from the Nd^{3+} ion to the activator given by Er^{3+} or Tm^{3+} [162]. This mechanism suffers from several drawbacks: i) Nd^{3+} concentration lower than 1% causes weak absorption events and, consequently, weak upconversion emission, ii) the presence of the Nd^{3+} sensitizer may cause direct quenching of the upconversion emission through energy back-transfer from the activators to Nd^{3+}.

5.4 Core-shell architectures

The above discussion and examples suggest a few main points to be accounted for in practice to overcome the limitations introduced by nanoscale resizing of upconverters.
Whereas lanthanide dopants usually occupy the lattice sites of the host cations, for increasing surface area, dopants may be found preferentially in surface and edge sites [163,164] , that causes a not statistical distribution of dopants and dispersed inter-dopant distance. Therefore, for increasing surface-to-volume ratio, it is natural to distinguish between the internal core region and outer surface region of a nanocrystal. This means that surfaces being responsible of upconversion luminescence quenching by trap states, structured design of the outer region of the nanocrystal, surfactants or proper chemically anchored surface organics can assist the activator-sensitizer interaction inside the nano-upconverter and, as a consequence, assist the upconversion luminescence [87,136].
In particular, the possibility offered by nanotechnology of fabricating specially structured nanocrystals with spatial separation between dopants (sensitizers and activators) has enabled to optimize the excitation energy migration and activator-sensitizer interactions by a rational design of doping [82]. In practice, advancement in fundamental knowledge and practical applications of nano-upconverters has been prompted by progress in nanoscale synthesis and processing approaches [39,40]. For instance, since ultrahigh sensitive fluorescent label for biomolecule imaging demands sub 10 nm-size efficiently emitting upconverters, particular attention has to be paid to synthesis approaches to obtain state of art structural order, control on size-dispersion and composition for ultrasmall nanoparticles [33,39]. Rational design of the doping to optimize activator-sensitizer interactions, in the presence of closely matched intermediate-excited states, and inter-dopant spacing are important in modulating energy transfer processes, luminescence performances and finally upconversion efficiency of nano-upconverters [165,166].
A commonly used strategy for enhancing the upconversion luminescence of nano-phosphors is the synthesis of core-shell nanocrystals where inert shell passivation as well as different dopants for the core and the shell regions enable to induce spatially confined energy transfer processes [82]. Efficient upconversion emission (seven times larger than the conventional activator-sensitizer doped host system) under 808 nm excitation relies on the spatial separation of the two sensitizers by a core-shell design of the nanocrystal letting to increase the doping concentration of the Nd^{3+} sensitizer without the deleterious quenching Nd^{3+}-Nd^{3+} interaction. In practice, $NaGdF_4$ host can be doped by Yb^{3+} and activator Er^{3+} in the core region of the nanocrystal (where the Yb^{3+}-sensitized upconversion occurs) and by Nd^{3+}-Yb^{3+} in the shell region (where Nd^{3+} excitation and Nd^{3+} to Yb^{3+} energy transfer takes place) [167]. The above example points out the occurrence of "long-range" interaction process named "energy-migration-mediated upconversion [168] that differs from the ETU process for which the energy

of the excited states hops step-by-step in a random way from donor to donor until the acceptor ions trapping for upconversion emission. “Long-range” interaction means that the energy transfer pathway is not local in that the energy can be captured by an acceptor even for acceptor-donor spacing of several nanometers in the presence of an assisting ion (typically Gd and Yb). For instance, in a core-shell architecture of $NaGdF_4$ nanocrystals, the excitation energy is absorbed in the core region by Yb^{3+}-Tm^{3+} upconversion processes followed by $Tm^{3+} \rightarrow Gd^{3+}$ energy transfer and, subsequently, random hopping of the energy between Gd ions of the middle layer makes possible capture of the energy from the acceptor ions (Eu^{3+}/Tb^{3+}/Sm^{3+}/Dy^{3+} doping the shell region [168]. In addition to Gd ions, long-range energy transfer can be supported by Yb^{3+} in core-active shell architectures [168-170].

A distribution of Yb^{3+} ions with very high content (98 mol%) properly arranged in terms of order and structure in an orthorhombic lattice (i.e., Er^{3+}(2%)-doped nanocrystals with orthorhombic lattice structure doped with Yb^{3+} ions distributed in arrays of clusters) were found to generate a four-photon-promoted violet up-conversion very intense emission from Er^{3+} ions [51]. Through this particular design, Yb^{3+}- Yb^{3+} energy transfer is confined and energy transfer to defects is minimized, thus leading to an unconventional very intense four-photon-promoted violet upconversion emission from Er^{3+}.

As a further example, a LaF_3 core–shell system with Eu^{3+}-doped core and Tb^{3+}-doped shell separated by an undoped LaF_3 shell enables control of the energy transfer between Eu^{3+} and Tb^{3+} and the Tb^{3+}/ Eu^{3+} emission ratio by variation of the thickness of the LaF_3 shell [171-173]. Multilayered core-shell-shell structured lanthanide doped $NaYF_4$ nanoparticles with spatially separated Er^{3+} activators and Yb^{3+} sensitizers were demonstrated to yield enhanced multi-photon emission from Er^{3+} in the presence of an interlayer between activator-doped core and sensitizer-doped shell assisting the excitation energy transfer [174]. This architecture accomplishes suppression of the concentration quenching limitation acting on the cross-relaxation between the activator and the sensitizer and exhibits high quantum yield (up to 6.34 %).

Definitively, for a critical distance (Förster critical distance) in the range of 2−6 nm [175], or doping content below 10^{-2} M for [160], brighter luminescent nanocrystals can be obtained under optimized composition, architecture and excitation-emission schemes [90,143,150,176-178].

Various approaches developed to control the negative impact of concentration quenching in homogeneously doped nanocrystals and core-shell nanostructures (designed to enable surface modification with protecting shells and local separation of dopants) in the presence of rare earth activator-sensitizers are overviewed in Ref [82].

To summarize the core−shell design principle, three main categories can be individuated: (Figure 10): i) passive-shell design, where dopants are incorporated in the core region of the nanocrystal [179], ii) active-shell design, where different dopants are incorporated in the core and shell regions [180], and iii) energy migration core−shell design with a core-shell-shell architecture where an optically active sub-lattice mediates the energy transfer processes through the core−shell interface [168].

Core/inert shell or core/active shell design with optimized lanthanide concentration and suitable crystal phase/symmetry of the host lattice or presence of enhanced plasmonic fields are useful strategies to enhance upconversion luminescence efficiency by several orders of magnitudes via control on the intermediate energy transfer mechanisms [32]. Typically nano-upconverters including Yb^{3+}ions, that absorb IR radiation and nonradiatively transfer the acquired excitation to another lanthanide ion (such as, Er^{3+}, Ho^{3+}, or Tm^{3+}) that emits visible or ultraviolet by upconversion, may have limits in producing bright upconversion due to both narrow IR absorption spectral window (10 260–10 660 cm^{-1}) and small absorption cross-section of Yb^{3+} dopants [181]. An alternative emerged in recent years is using organic dyes, to enhance the brightness of core-shell nano-upconverters by up to 3000 times for sub-20 nm particles in the absence of inert shell passivation [182].

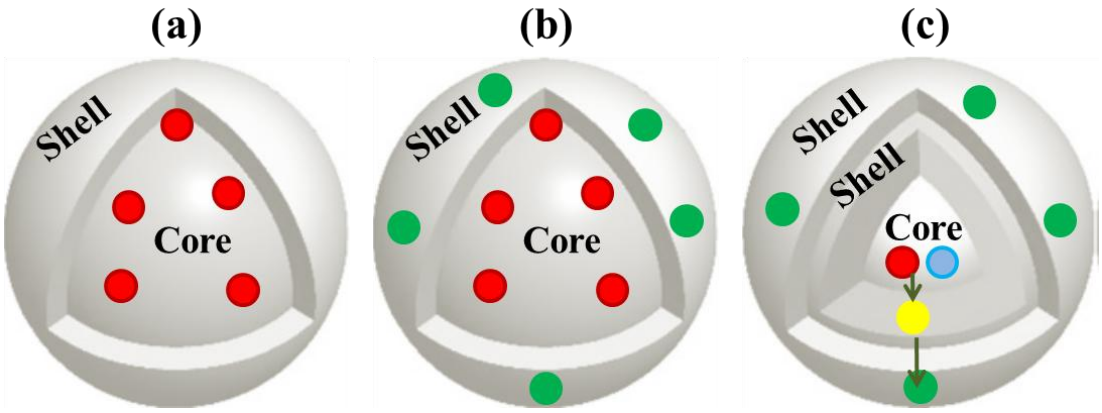

Figure 10: Schematics of the most common core-shell architectures: (a) passive-shell design, (b) active-shell coating design with different dopants in the core and shell regions, and (c) energy transfer core−shell design with core-shell-shell architecture).

Additionally, plasmon-mediated upconversion enhancement (i.e., the amplification in local electromagnetic field by coupling noble metals) is another emerging field of research in applicative frameworks demanding low-power irradiance, such as upconversion-mediated photovoltaics and bioimaging [42,43,183,184]. The theoretical origin of an upconversion enhancement in the presence of surface plasmon resonance was overviewed not recently [185-187]. The luminescence enhancement is mostly ascribed to the intensification of the electric field intensity close to the noble metal nanoparticle's surface that can reinforce the absorption of the nano-upconverters and the emission of the activators as well as affect the nonradiative transition rates. In practice, a critical parameter for the plasmonic enhancement effect is the positional relation between emitters and metallic surfaces or particles [188,189] that needs specifically and optimally designed structure and shape of the plasmonic material [43,190,191].

Reported approaches to enhance the upconversion emission of nanoparticles using a plasmonic field consist of setting the plasmonic resonance with upconversion emissions [188] [192]and setting the plasmonic resonance with the excitation wavelength of the upconversion emission. Assembly of nanophosphors with different chemistry and coupling between plasmon nanoparticles and lanthanide-activated nanophosphors [193] provides interesting input for the optimum design of future hybrid nanoupconverters and metal nanostructures.

Another very active research field of nano-upconverters is lighting with fine tuning of the color output and multicolor emission by single wavelength excitation allowed by the f energy levels of lanthanides hardly affected by the chemical environment and balanced overlap of the emission from several lanthanide dopants [45]. In the field of white light emission for indoor and outdoor lighting, common strategies to design white light emitting diodes (LEDs) relies on either combining blue LED and yellow phosphors or mixing red, green and blue emissions from phosphors excited with an UV or IR source (RGB phosphors). In this case a single host crystal is preferred and multicolor emission is provided by a single rare earth-dopant able of multiple output colors (Sm^{3+}, Eu^{3+} or Dy^{3+}), by lanthanide co-dopants (for instance, Ce^{3+}/Mn^{2+}, Ce^{3+}/Tb^{3+}, Ce^{3+}/Ho^{3+}, Tb^{3+}/Sm^{3+} pairs etc.) exchanging energy via energy transfer or multiple dopants emitting different colors ($Ce^{3+}/Li^{+}/Mn^{2+}$, $Eu^{3+}/Tb^{3+}/Tm^{3+}$, $Eu^{2+}/Tb^{3+}/Eu^{3+}$) [194].

5.5 Excited state dynamics

Further important implications of the spatial confinement of lanthanide dopants are i) the impact on the spectroscopic dynamic quantities, such as probability of either radiative or non-radiative transitions, lifetime of the rare earth's intermediate states, thermal line broadening and thermal line shifting [195-197], and ii) changes in the density of states (DOS) of phonons [154].

As already outlined, depending on the energy mismatch, excited states can relax their energy via photon emission or phonon emission.

In nanocrystals the radiative decay rate may change due to two main effects. First, the impact of size- and surrounding-related modification of the refractive index [195,196]. In this case, the Judd-Ofelt formula should be properly modified. To detail, based on the Judd-Ofelt theory, the rate of radiative relaxation from an initial state I_i to a final state I_f can be expressed as follows:

$$W_R\ I_i,I_f\ = \frac{64\ \pi^2 \Delta E^2}{3h\ (2I_i+1)}\ \ \chi F^2+n_h^3 M^2$$

where ΔE (cm^{-1}) is the energy gap between the states involved in the transition, F^2 is the matrix element of the electric dipole moments, M^2 is the matrix element of the magnetic dipole moment, n_h is the refractive index of the host crystal, and $\chi = n_h\ (n_h^2+2)^2/9$ is a corrective factor for the local field (the so-called Lorentz correction) [198,199]. For nanocrystals with average size much shorter than the exciting wavelength, an effective refractive index has to be considered, that is $n_{eff}(x)=x*n_{NP}+(1-x)*n_d$, where x is a filling factor accounting for the effective volume occupied by the nanoparticles, n_{NP} is the refractive index of the material of the nanocrystal and n_d is the refractive index of the dielectric surrounding/embedding the nanocrystals. The radiative lifetime may be calculated by the Judd-Ofelt theory under the approximation that the average size of the nanoparticles is much shorter than the exciting wavelength (sub-wavelength regime).

Second, field oscillations due to coherent interference between exciting field and lattice electrostatic field along the radius of the emitting nanocrystals were found to inhibit spontaneous emission from nanocrystals with size ranging from 100 nm to 2 μm and embedded in different dielectric media [196,197].

Turning to the non-radiative decay rate, in homogeneous crystals it decays exponentially according to the "gap rule" exp ($-A_{host}$ p), where A_{host} is a parameter associated with the host material and $p=\Delta E/\Delta E_{ph}$ is the number of phonons required to bridge the energy gap ΔE between the initial and final states involved in the transition. According to a picture in which a nanoparticle is separated into a spherical internal core and a near-surface shell region, the contribution of the near surface region to the decay rate increases for decreasing nanocrystal size. The maximum vibrational energy ΔE_{ph} is a key quantity involved in non radiative channels stemming from the nanocrystal core region (where phonon modes are the intrinsic ones), surface ligands (vibrational spectrum of the nanocrystal surface), surrounding-mediated quenching and defect species and density [139] . A high density of defects yields reduced lifetime according to the Stern-Volmer relationship [200], that is proportionally to the quenching rate constant and the density of quenching defects.

From the practical standpoint, increased surface-to-volume ratio implies lowered strength of the crystal field around the surface dopant-site, luminescence quenching through surface defects and phonon-assisted relaxations, excitation transfer from inner to surface atoms, differences between surface and core luminescent centers, increasing fraction of surface dopants and decreasing number of active centers [97]. In addition to such effects that can be argued experimentally, fundamental insight in the differences between bulk and nanoscale radiationless processes can be gained by considering the changes in the phonon density of states resulting from the spatial confinement.

Spectroscopy of bulk phosphors states that while inhomogeneous broadening of a spectral line can result from defects and non-uniform shift of the electronic energy levels, homogeneous broadening is

related to temperature-dependent phonon coupling (weak ion-phonon coupling). If the phonon density of states (DOS) is a Debye distribution, the temperature-dependent line-width (ΔE) and line-shift (δE) can be expressed by the McCumber-Sturge formulas [201]

$$\Delta E\ T\ (cm^{-1}) = \Delta E_o + \alpha \left(\frac{T}{T_D}\right)^7 \int_0^{T_D/T} \frac{x^6 e^x}{(e^x-1)^2} dx$$

$$\delta E\ T\ (cm^{-1}) = \alpha \left(\frac{T}{T_D}\right)^4 \int_0^{T_D/T} \frac{x^3}{e^x-1} dx$$

where ΔE_0 refers to a residual line-width at very low temperatures, α and α are coefficients related to the electron-phonon coupling, and $T_D=h\upsilon_D/k$ (υ_D is the Debye cut-off frequency of the lattice and k is the Boltzmann constant) is the effective Debye temperature of the phonon distribution.

Going from bulk to nanosized crystals, the McCumber-Sturge formulas are no longer valid because phonon DOS turns from a continuous (Debye approximation) to a discrete distribution with size-dependent cutoff frequency [154,156,202,203]. Moreover, vibronic effects may become strong and dominant [60,204,205]. Consequences of the spatial confinement on the electron-phonon coupling are: i) modified temperature-dependence (T^3 instead of T^7) of the linewidth for the characteristic transitions of Eu^{3+} in Y^2O^3 nanoparticles [206], ii) lifetime increased from 220 ns to 27 μs of a multiplet of Eu^{3+} in Y_2O_3 turning from the bulk to the nano-sized material [207] , and iii) size-dependent removal of direct phonon relaxation in Er^{3+}-doped Y_2O_2S nanocrystals (anomalous thermalization) [156].

Turning back to the size-related characteristics of the phonon DOS, since high frequency phonon DOS is unaffected by the spatial confinement, any radiationless decay involving high-frequency phonons is not size-sensitive. Differently, depending on the energy mismatch between the states involved in a phonon-assisted decay, a restricted number of phonon modes due to size scaling down causes constraints in the presence of a small energy gap and no significant effects if the energy gap is close to or higher than the Debye energy of the lattice. Importantly, changes in the low-frequency acoustic phonon DOS induced by the spatial confinement impact even on the highly localized and shielded 4f states of lanthanide ions because of the cutoff in low frequency phonon modes [208,209]. Very interestingly, efficiently luminescent nano-upconverters were demonstrated in some oxide compounds with suitable phonon thresholds: in Er^{3+}-Yb^{3+} co-activated cubic Y_2O_3, tetragonal $GdVO_4$ and tetragonal $NaGd(WO_4)_2$ (which have different phonon thresholds, 600 cm^{-1}, 880 cm^{-1} and 1000 cm^{-1}) micro-sized powders, the visible upconversion luminescence of Er^{3+} relative to near-infrared emissions increases remarkably (120-fold) with the increase of phonon thresholds [210].

A further phenomenon affected by the size-dependent phonon DOS is anomalous thermalization due to the possible differences between nonradiative relaxation of ions from excited electronic states in nanocrystals and bulk counterpart material [36].

Therefore, as a consequence of the removal of low frequency phonons, i) losses are reduced by suppression of the complete direct phonon relaxation between levels with energy gap lower than the cutoff phonon frequency, ii) non-radiative relaxation between states with energy mismatch smaller (larger) than the Debye energy of the lattice are size-dependent (size-independent), iii) thermal relaxation is size-dependent because radiationless depopulation of an excited lanthanide state may be inhibited by the absence of low-energy phonon states [156,211] and iv) a fastly decaying level in bulk materials could live long enough to decay radiatively rather than by one-phonon emission.

Emission decay patterns also present a dependence on size and size-distribution. Litetimes of the 4f–4f transitions of lanthanides range from microseconds to milliseconds and an be tuned by the concentration in a local environment. The lifetime or radiative decay time τ, that is the inverse of the probability of the transition of interest (given as the sum of several probabilities related to radiative and non-radiative independent processes), of an optical center in bulk phosphors enters in the decay curves through the following mono-exponential decay formula:

$$I = I_0 \exp^{-t}{}_{\tau}$$

where I and I_0 are the luminescence intensities at times t and initial (set to zero), respectively. In lanthanide-activated nanocrystals, the decay patterns of the luminescent ions can exhibit multi-exponential decay dependence due to the presence and interplay of several contributions, such as intrinsic phonon modes, vibration energy of surface ligands, solvent-mediated quenching, different probability of the radiationless decay of surface ions and core ions, adsorbed surface water, surface defects, inhomogeneous distribution of dopants throughout the nanoparticle volume [139,212,213]. For decreasing particle size, the decay time can be enhanced or decreased depending on the doping content [214-216]. Single-exponential decay profiles with a lifetime comparable to that of the un-doped host can be found for large ion-ion spatial distance (diluted doping conditions). On the other hand, a non-exponential decay behavior of the photoluminescence intensity was reported for raised doping level of the luminescent ions [217]. Also, an enhancement of the excitation intensity can imply a non-exponential decay time and shortening of the effective average decay times [218]. Noteworthy, the issue of the control and fine tuning of the lifetimes of the f-f transitions of lanthanides has been demonstrated by a is a pioneering discovery focusing on the transient state rather than the steady state of such electronic transitions [125]. More than ten nanocrystal populations with distinct lifetimes ranging from 25.6 μs to 662.4 μs were reported and identified by a single color band.
Further size-dependent spectroscopic quantities are broadening and shifting of the spectral lines in the limit of low temperatures and very small particles (much smaller than 50 nm) [154]

6. Conclusions

In conclusion, physics of phosphors has been overviewed starting from the basic knowledge, i.e., the main radiative and non-radiative mechanisms, down-conversion and upconversion processes, rare earth dopants and their role as luminescence centers in simply and co-doped host crystals, the building-block dopant-dopant interaction pathways and quenching phenomena. Then, the discussion has remarked important differences between nanophosphors and bulk phosphors in regard to **i)** the relevance of the surface-to-volume ratio, surface chemistry and composition as well as strength of coordination, **ii)** effects of the spatial confinement on rare earth emission, **iii)** role of the content of the emitting centers and proper choice of the co-dopants on the output color tuning, pathways leading to upconversion luminescence and upconversion yield, i**v)** changes of the density of state of phonons resulting from nanoscale resizing (introduction of a discrete distribution of the phonon energy states with a low energy phonon cutoff), and **v)** dynamical quantities, such as probability of radiative and non-radiative transitions, lifetime of the excited states, thermal line broadening and thermal line shifting) are affected by the nanoscale-regime). Moreover, relevant differences between nanophosphors and semiconductor quantum dots have been detailed that also clarify the advantages of using nano-upconverters in many applications. Indeed, whereas the field of nanophosphors is a knowledge in progress, meaning that our present comprehension of their physics and properties is still incomplete, more and more attention is being drawn to the unique properties of lanthanide doped nano-upconverters owing to promising applications in place. For instance, nano-upconverters find relevant applications in biological and biomedical fields, fluorescence microscopy, super-resolution imaging and single-molecule sensing that require bright emission from nanometer-sized crystals. The transformation of the upconversion mechanisms exhibited by nanophophors into real-world applications has been made possible by the relevant progresses in nanofabrication and wet-synthesis methods combined with proper choice of materials (host and lanthanide dopants) and architectures (such as, core-shell design) to improve the upconversion efficiency. The remarkable applicative interest is also having benefits in terms of fundamental investigation of the impact of the spatial confinement on the physics of phosphors.

Definitively, lanthanide-activated nano-upconverters have a great potential in pushing both theoretical knowledge and applicative performances in recent challenging application fields to a new level.

List of abbreviations

Activator , A
Cross-relaxation, CR
Energy migration upconversion, EMU
Energy transfer, ET
Energy transfer upconversion, ETU
Excited state absorption, ESA
Full width at half maximum, FWHM
Ground state absorption, GSA
Infrared, IR
Photon avalanche, PA
Sensitizer, S
Two photon absorption, TPA
Two-photon excited state absorption, 2-ESA
Ultraviolet, UV
Yttrium aluminum garnet, YAG

References

1. Wiedemann, E. Ueber Fluorescenz und Phosphorescenz I. Abhandlung. *Annalen der Physik* **1888**, *270*, 446-463.
2. Virk, H. S. History of Luminescence from Ancient to Modern Times, *Defect and diffusion Forum* **2014**, 361, 1-13.
3. Lastusaari, M.; Bettinelli, M.; Eskola, K.; Hölsä, J.; Jungner, H.; Kotlov, A.; Laamanen, T.; Malkamäki, M.; Welter, E.; Holsa, J., et al. The Bologna Stone: History's First Persistent Luminescent Material. *European Journal of Mineralogy* **2012**, *24*.
4. Wang, J.; Tanner, P.A. Upconversion for White Light Generation by a Single Compound. *Journal of the American Chemical Society* **2010**, *132*, 947-949.
5. Pollnau, M.; Gamelin, D.R.; Lüthi, S.R.; Güdel, H.U.; Hehlen, M.P. Power dependence of upconversion luminescence in lanthanide and transition-metal-ion systems. *Physical Review B* **2000**, *61*, 3337-3346.
6. Valeur, B.; Berberan-Santos, M.N. A Brief History of Fluorescence and Phosphorescence before the Emergence of Quantum Theory. *Journal of Chemical Education* **2011**, *88*, 731-738.
7. Miyakawa, T.; Dexter, D.L. Phonon Sidebands, Multiphonon Relaxation of Excited States, and Phonon-Assisted Energy Transfer between Ions in Solids. *Physical Review B* **1970**, *1*, 2961-2969.
8. Judd, B.R. Optical Absorption Intensities of Rare-Earth Ions. *Physical Review* **1962**, *127*, 750-761.
9. Ofelt, G.S. Intensities of Crystal Spectra of Rare-Earth Ions. *The Journal of Chemical Physics* **1962**, *37*, 511-520.
10. Riseberg, L.A.; Moos, H.W. Multiphonon Orbit-Lattice Relaxation of Excited States of Rare-Earth Ions in Crystals. *Physical Review* **1968**, *174*, 429-438.
11. May, P.S.; Baride, A.; Hossan, M.Y.; Berry, M. Measuring the internal quantum yield of upconversion luminescence for ytterbium-sensitized upconversion phosphors using the ytterbium(iii) emission as an internal standard. *Nanoscale* **2018**, *10*, 17212-17226.
12. Bloembergen, N. Solid State Infrared Quantum Counters. *Physical Review Letters* **1959**, *2*, 84-85.

13. Porter, J.F. Fluorescence Excitation by the Absorption of Two Consecutive Photons. *Physical Review Letters* **1961**, *7*, 414-415.
14. Boulon, G. Fifty years of advances in solid-state laser materials. *Optical Materials* **2012**, *34*, 499-512.
15. dos Santos, P.V.; de Araujo, M.T.; Gouveia-Neto, A.S.; Medeiros Neto, J.A.; Sombra, A.S.B. Optical temperature sensing using upconversion fluorescence emission in Er^{3+}/Yb^{3+}-codoped chalcogenide glass. *Applied Physics Letters* **1998**, *73*, 578-580.
16. Auzel, F. Compteur quantique par transfert d'energie entre deux ions de terres rares dans un tungstate mixte et dans un verre. *C. R. Acad. Sci. Paris* **1966**, *262*, 1016-1019.
17. Auzel, F. Quantum counter by energy transfer from Yb3+ to Tm3+ in a mixed tungstate and a germanate glass. C. R. Acad. Sci. **1966**, 263, 819−821
18. Suyver, J.F.; Aebischer, A.; Biner, D.; Gerner, P.; Grimm, J.; Heer, S.; Krämer, K.W.; Reinhard, C.; Güdel, H.U. Novel materials doped with trivalent lanthanides and transition metal ions showing near-infrared to visible photon upconversion. *Optical Materials* **2005**, *27*, 1111-1130.
19. Nadort, A.; Zhao, J.; Goldys, E.M. Lanthanide upconversion luminescence at the nanoscale: fundamentals and optical properties. *Nanoscale* **2016**, *8*, 13099-13130.
20. Auzel, F. Upconversion and Anti-Stokes Processes with f and d Ions in Solids. *Chemical Reviews* **2004**, *104*, 139-174.
21. Liu, G.; Chen, X. Properties of Lanthanides in Nano-materials in *Handbook on the Physics and Chemistry of Rare Earths*; Gschneidner, J.K.A.; Eyring, L.; Pecharsky Eds, V. North Holland, Elsevier **2007**; Vol. 37, pp 99–169,
22. Dieke, G.H.; Crosswhite, H.M.; Crosswhite, H. *Spectra and energy levels of rare earth ions in crystals*; Interscience Publishers: New York, **1968**.
23. Cesaria, M.; Di Bartolo, B. Nanophosphors: from rare earth activated multicolor-tuning to new efficient white light sources in . Book Quantum Nano-Photonics, NATO Science for Peace and Security Series B: Physics and Biophysics, Springer, Berlin, **2018** and references therein.
24. Chang, N.C.; Gruber, J.B. Spectra and Energy Levels of Eu^{3+} in Y_2O_3. *The Journal of Chemical Physics* **1964**, *41*, 3227-3234.
25. Buijs, M.; Meyerink, A.; Blasse, G. Energy transfer between Eu^{3+} ions in a lattice with two different crystallographic sites: $Y_2O_3:Eu^{3+}$, $Gd_2O_3:Eu^{3+}$ and Eu_2O_3. *Journal of Luminescence* **1987**, *37*, 9-20.
26. Dorenbos, P. 5d-Level Energies of Ce^{3+} and the Crystalline Environment. I. Fluoride Compounds. *Physical Review B - Condensed Matter and Materials Physics, 62 (23)* **2000**, *62*.
27. Dorenbos, P. 5d-Level Energies of Ce^{3+} and the Crystalline Environment. II. Chloride, Bromide, and Iodide Compounds. *Physical Review B - Condensed Matter and Materials Physics, 62 (23)* **2000**, *62*.
28. Dorenbos, P. 5d-Level Energies of Ce^{3+} and the Crystalline Environment. III. Oxides Containing Ionic Complexes. *Physical Review B - Condensed Matter and Materials Physics, 64* **2001**, *64*,.
29. Tu, D.; Liu, Y.; Zhu, H.; Li, R.; Liu, L.; Chen, X. Breakdown of Crystallographic Site Symmetry in Lanthanide-Doped $NaYF_4$ Crystals. *Angewandte Chemie International Edition* **2013**, *52*, 1128-1133, 8.
30. Yi, Z.; Lu, W.; Xu, Y.; Yang, J.; Deng, L.; Qian, C.; Zeng, T.; Wang, H.; Rao, L.; Liu, H., et al. PEGylated $NaLuF_4$: Yb/Er upconversion nanophosphors for in vivo synergistic fluorescence/X-ray bioimaging and long-lasting, real-time tracking. *Biomaterials* **2014**, *35*, 9689-9697.
31. Krämer, K.W.; Biner, D.; Frei, G.; Güdel, H.U.; Hehlen, M.P.; Lüthi, S.R. Hexagonal Sodium Yttrium Fluoride Based Green and Blue Emitting Upconversion Phosphors. *Chemistry of Materials* **2004**, *16*, 1244-1251.
32. Li, X.; Zhang, F.; Zhao, D. Lab on upconversion nanoparticles: optical properties and applications engineering via designed nanostructure. *Chemical Society Reviews* **2015**, *44*, 1346-1378.
33. Gai, S.; Li, C.; Yang, P.; Lin, J. Recent Progress in Rare Earth Micro/Nanocrystals: Soft Chemical Synthesis, Luminescent Properties, and Biomedical Applications. *Chemical Reviews* **2014**, *114*, 2343-2389.
34. Zhu, X.; Zhang, J.; Liu, J.; Zhang, Y. Recent Progress of Rare-Earth Doped Upconversion Nanoparticles: Synthesis, Optimization, and Applications. *Advanced Science* **2019**, *6*, 1901358 and references therein.

35. Sun, L.-D.; Dong, H.; Zhang, P.-Z.; Yan, C.-H. Upconversion of Rare Earth Nanomaterials. *Annual Review of Physical Chemistry* **2015**, *66*, 619-642.
36. Liu, G. Advances in the theoretical understanding of photon upconversion in rare-earth activated nanophosphors. *Chemical Society Reviews* **2015**, *44*, 1635-1652 and references therein.
37. Feng, W.; Han, C.; Li, F. Upconversion-Nanophosphor-Based Functional Nanocomposites. *Advanced Materials* **2013**, *25*, 5287-5303.
38. Li, X.; Zhang, F.; Zhao, D. Highly efficient lanthanide upconverting nanomaterials: Progresses and challenges. *Nano Today* **2013**, *8*.
39. Wang, F.; Han, Y.; Lim, C.S.; Lu, Y.; Wang, J.; Xu, J.; Chen, H.; Zhang, C.; Hong, M.; Liu, X. Simultaneous phase and size control of upconversion nanocrystals through lanthanide doping. *Nature* **2010**, *463*, 1061-1065.
40. Liu, D.; Xu, X.; Du, Y.; Qin, X.; Zhang, Y.; Ma, C.; Wen, S.; Ren, W.; Goldys, E.M.; Piper, J.A., et al. Three-dimensional controlled growth of monodisperse sub-50 nm heterogeneous nanocrystals. *Nature Communications* **2016**, *7*, 10254.
41. Han, S.; Deng, R.; Xie, X.; Liu, X. Enhancing Luminescence in Lanthanide-Doped Upconversion Nanoparticles. *Angewandte Chemie International Edition* **2014**, *53*, 11702-11715.
42. Xu, W.; Chen, X.; Song, H. Upconversion manipulation by local electromagnetic field. *Nano Today* **2017**, *17*, 54-78.
43. Das, A.; Mao, C.; Cho, S.; Kim, K.; Park, W. Over 1000-fold enhancement of upconversion luminescence using water-dispersible metal-insulator-metal nanostructures. *Nature Communications* **2018**, *9*, 4828.
44. Wu, S.; Xia, H.; Xu, J.; Sun, X.; Liu, X. Manipulating Luminescence of Light Emitters by Photonic Crystals. *Advanced Materials* **2018**, *30*, 1803362.
45. Cesaria, M.; Di Bartolo, B. Nanophosphors-Based White Light Sources. *Nanomaterials* **2019**, *9*, 1048 and references therein.
46. Gedanken, A.; Reisfeld, R.; Sominski, L.; Zhong, Z.; Koltypin, Y.; Panczer, G.; Gaft, M.; Minti, H. Time-dependence of luminescence of nanoparticles of Eu_2O_3 and Tb_2O_3 deposited on and doped in alumina. *Applied Physics Letters* **2000**, *77*, 945-947.
47. Görller-Walrand, C.; Binnemans, K.; Handbook on the Physics and Chemistry of Rare Earths, Gscheidner Jr., K.A.; Eyring, L. Eds; **1996**, Elsevier Science B.V. vol. 23, pp. 121–283.
48. van Dijk, J.M.F.; Schuurmans, M.F.H. On the nonradiative and radiative decay rates and a modified exponential energy gap law for 4f–4f transitions in rare-earth ions. *The Journal of Chemical Physics* **1983**, *78*, 5317-5323.
49. Vleck, J.H.V. The Puzzle of Rare-earth Spectra in Solids. *The Journal of Physical Chemistry* **1937**, *41*, 67-80.
50. Gamelin D.R., G.H.U. Upconversion processes in transition metal and rare earth metal systems. In *ransition Metal and Rare Earth Compounds. Topics in Current Chemistry*, H., Y., Ed. Springer: Berlin, 2001; Vol. 214, p. 1.56.
51. Wang, J.; Deng, R.; MacDonald, M.A.; Chen, B.; Yuan, J.; Wang, F.; Chi, D.; Andy Hor, T.S.; Zhang, P.; Liu, G., et al. Enhancing multiphoton upconversion through energy clustering at sublattice level. *Nature Materials* **2014**, *13*, 157-162.
52. Thoma, R.E.; Insley, H.; Hebert, G.M. The Sodium Fluoride-Lanthanide Trifluoride Systems. *Inorganic Chemistry* **1966**, *5*, 1222-1229.
53. Shang, M.; Li, G.; Kang, X.; Yang, D.; Geng, D.; Peng, C.; Cheng, Z.; Lian, H.; Lin, J. LaOF : Eu3+ nanocrystals: hydrothermal synthesis, white and color-tuning emission properties. *Dalton Transactions* **2012**, *41*, 5571-5580.
54. den Engelsen, D.; Fern, G.R.; Ireland, T.G.; Harris, P.G.; Hobson, P.R.; Lipman, A.; Dhillon, R.; Marsh, P.J.; Silver, J. Ultraviolet and blue cathodoluminescence from cubic Y_2O_3 and Y_2O_3:Eu^{3+} generated in a transmission electron microscope. *Journal of Materials Chemistry C* **2016**, *4*, 7026-7034,.
55. Güdel, H.U.; Pollnau, M. Near-infrared to visible photon upconversion processes in lanthanide doped chloride, bromide and iodide lattices. *Journal of Alloys and Compounds* **2000**, *303-304*, 307-315.
56. Sommerdijk J.L., B., A. Philips technical review. **1974**, 34, 24-32.

57. Förster, T. Energy migration and fluorescence. *Journal of biomedical optics* **2012**, *17*, 011002,
58. Axe, J.D.; Weller, P.F. Fluorescence and Energy Transfer in Y_2O_3:Eu^{3+}. *The Journal of Chemical Physics* **1964**, *40*, 3066-3069.
59. Liu, X.; Qiu, J. Recent advances in energy transfer in bulk and nanoscale luminescent materials: from spectroscopy to applications. *Chemical Society Reviews* **2015**, *44*, 8714-8746.
60. Tanner, P.A.; Zhou, L.; Duan, C.; Wong, K.-L. Misconceptions in electronic energy transfer: bridging the gap between chemistry and physics. *Chemical Society Reviews* **2018**, *47*, 5234-5265.
61. Forster, T. Zwischenmolekulare Energiewanderung und Fluoreszenz. Ann. Phys. **1948**, 437, 55-75.
62. Dexter, D.L. A Theory of Sensitized Luminescence in Solids. *The Journal of Chemical Physics* **1953**, *21*, 836-850.
63. You, Z.-Q.; Hsu, C.-P.; Fleming, G.R. Triplet-triplet energy-transfer coupling: Theory and calculation. *The Journal of Chemical Physics* **2006**, *124*, 044506.
64. Edvardsson, S.; Wolf, M.; Thomas, J.O. Sensitivity of optical-absorption intensities for rare-earth ions. *Physical Review B* **1992**, *45*, 10918-10923.
65. Ganem, J.; Crawford, J.; Schmidt, P.; Jenkins, N.W.; Bowman, S.R. Thulium cross-relaxation in a low phonon energy crystalline host. *Physical Review B* **2002**, *66*, 245101.
66. Pandozzi, F.; Vetrone, F.; Boyer, J.-C.; Naccache, R.; Capobianco, J.A.; Speghini, A.; Bettinelli, M. A Spectroscopic Analysis of Blue and Ultraviolet Upconverted Emissions from $Gd_3Ga_5O_{12}$:Tm^{3+}, Yb^{3+} Nanocrystals. *The Journal of Physical Chemistry B* **2005**, *109*, 17400-17405.
67. Yamada, N.; Shionoya, S.; Kushida, T. Phonon-Assisted Energy Transfer between Trivalent Rare Earth Ions. *Journal of the Physical Society of Japan* **1972**, *32*, 1577-1586.
68. Auzel, F. Multiphonon-assisted anti-Stokes and Stokes fluorescence of triply ionized rare-earth ions. *Physical Review B* **1976**, *13*, 2809-2817
69. Snitzer, E.; Woodcock, R. Yb^{3+}–Er^{3+} GLASS LASER. *Applied Physics Letters* **1965**, *6*, 45-46.
70. Wyatt, R. Spectroscopy of rare earth doped fibres. Proc. SPIE **1989**, 1171, 54–64.
71. Stokowski, S., E,. *Nd-doped Laser Glass Spectroscopic and Physical Properties*; Lawrence Livermore National Laboratory, University of California. **1981**; Vol. M-95, Rev. 2.
72. Jackson, S.D. Towards high-power mid-infrared emission from a fibre laser. *Nature Photonics* **2012**, *6*, 423-431.
73. Chen, G.; Liu, H.; Somesfalean, G.; Liang, H.; Zhang, Z. Upconversion emission tuning from green to red in Yb^{3+}/Ho^{3+}-codoped $NaYF_4$ nanocrystals by tridoping with Ce^{3+}ions. *Nanotechnology* **2009**, *20*, 385704,.
74. Gomes, L.; Courrol, L.C.; Tarelho, L.V.G.; Ranieri, I.M. Cross-relaxation process between +3 rare-earth ions in $LiYF_4$ crystals. *Physical Review B* **1996**, *54*, 3825-3829.
75. Igoshin, O.A.; Burshtein, A.I. Quenching of fluorescence by irreversible energy transfer at arbitrary strong pumping light. *Journal of Luminescence* **2000**, *92*, 123-132.
76. Szabo, A. Theory of diffusion-influenced fluorescence quenching. *The Journal of Physical Chemistry* **1989**, *93*, 6929-6939.
77. Danielmeyer, H.G.; Blätte, M.; Balmer, P. Fluorescence quenching in Nd:YAG. *Applied physics* **1973**, *1*, 269-274.
78. Dexter, D.L.; Schulman, J.H. Theory of Concentration Quenching in Inorganic Phosphors. *The Journal of Chemical Physics* **1954**, *22*, 1063-1070.
79. Auzel, F. A fundamental self-generated quenching center for lanthanide-doped high-purity solids. *Journal of Luminescence* **2002**, *100*, 125-130.
80. Zhang, H.; Li, Y.; Lin, Y.; Huang, Y.; Duan, X. Composition tuning the upconversion emission in $NaYF_4$:Yb/Tm hexaplate nanocrystals. *Nanoscale* **2011**, *3*, 963-966.
81. Mahalingam, V.; Vetrone, F.; Naccache, R.; Speghini, A.; Capobianco, J.A. Colloidal Tm3+/Yb3+-Doped $LiYF_4$ Nanocrystals: Multiple Luminescence Spanning the UV to NIR Regions via Low-Energy Excitation. *Advanced Materials* **2009**, *21*, 4025-4028.
82. Wen, S.; Zhou, J.; Zheng, K.; Bednarkiewicz, A.; Liu, X.; Jin, D. Advances in highly doped upconversion nanoparticles. *Nature Communications* **2018**, *9*, 2415.

83. Nakazawa, E.; Shionoya, S. Cooperative Luminescence in $YbPO_4$. *Physical Review Letters* **1970**, *25*, 1710-1712.
84. Chivian, J.S.; Case, W.E.; Eden, D.D. The photon avalanche: A new phenomenon in Pr^{3+}-based infrared quantum counters. *Applied Physics Letters* **1979**, *35*, 124-125.
85. Bednarkiewicz, A.; Chan, E.M.; Kotulska, A.; Marciniak, L.; Prorok, K. Photon avalanche in lanthanide doped nanoparticles for biomedical applications: super-resolution imaging. *Nanoscale Horizons* **2019**, *4*, 881-889E.
86. Suyver, J.F.; Grimm, J.; van Veen, M.K.; Biner, D.; Krämer, K.W.; Güdel, H.U. Upconversion spectroscopy and properties of $NaYF_4$ doped with Er^{3+}, Tm^{3+} and/or Yb^{3+}. *Journal of Luminescence* **2006**, *117*, 1-12.
87. Bai, X.; Song, H.; Pan, G.; Lei, Y.; Wang, T.; Ren, X.; Lu, S.; Dong, B.; Dai, Q.; Fan, L. Size-Dependent Upconversion Luminescence in Er^{3+}/Yb^{3+}-Codoped Nanocrystalline Yttria: Saturation and Thermal Effects. *The Journal of Physical Chemistry C* **2007**, *111*, 13611-13617.
88. Wang, F.; Liu, X. Recent advances in the chemistry of lanthanide-doped upconversion nanocrystals. *Chemical Society Reviews* **2009**, *38*, 976-989.
89. Dong, H.; Sun, L.-D.; Yan, C.-H. Basic understanding of the lanthanide related upconversion emissions. *Nanoscale* **2013**, *5*, 5703-5714.
90. Heer, S.; Kömpe, K.; Güdel, H.U.; Haase, M. Highly Efficient Multicolour Upconversion Emission in Transparent Colloids of Lanthanide-Doped $NaYF_4$ Nanocrystals. *Advanced Materials* **2004**, *16*, 2102-2105.
91. Zhou, B.; Shi, B.; Jin, D.; Liu, X. Controlling upconversion nanocrystals for emerging applications. *Nature Nanotechnology* **2015**, *10*, 924-936.
92. Alivisatos, A.P. Semiconductor Clusters, Nanocrystals, and Quantum Dots. *Science* **1996**, *271*, 933.
93. Wen, X.; Yu, P.; Toh, Y.-R.; Ma, X.; Tang, J. On the upconversion fluorescence in carbon nanodots and graphene quantum dots. *Chemical Communications* **2014**, *50*, 4703-4706.
94. Gan, Z.; Wu, X.; Zhou, G.; Shen, J.; Chu, P.K. Is There Real Upconversion Photoluminescence from Graphene Quantum Dots? *Advanced Optical Materials* **2013**, *1*, 554-558.
95. Blanton, S.A.; Hines, M.A.; Guyot-Sionnest, P. Photoluminescence wandering in single CdSe nanocrystals. *Applied Physics Letters* **1996**, *69*, 3905-3907.
96. Teitelboim, A.; Oron, D. Broadband Near-Infrared to Visible Upconversion in Quantum Dot–Quantum Well Heterostructures. *ACS Nano* **2016**, *10*, 446-452.
97. Abrams, B.L.; Holloway, P.H. Role of the Surface in Luminescent Processes. *Chemical Reviews* **2004**, *104*, 5783-5802.
98. Carlos, L.D.; Ferreira, R.A.S.; Bermudez, V.d.Z.; Ribeiro, S.J.L. Lanthanide-Containing Light-Emitting Organic–Inorganic Hybrids: A Bet on the Future. *Advanced Materials* **2009**, *21*, 509-534.
99. Gu, B.; Zhang, Q. Recent Advances on Functionalized Upconversion Nanoparticles for Detection of Small Molecules and Ions in Biosystems. *Advanced Science* **2018**, *5*, 1700609.
100. Sun, L.-D.; Wang, Y.-F.; Yan, C.-H. Paradigms and Challenges for Bioapplication of Rare Earth Upconversion Luminescent Nanoparticles: Small Size and Tunable Emission/Excitation Spectra. *Accounts of Chemical Research* **2014**, *47*, 1001-1009.
101. Zheng, W.; Huang, P.; Tu, D.; Ma, E.; Zhu, H.; Chen, X. Lanthanide-doped upconversion nano-bioprobes: electronic structures, optical properties, and biodetection. *Chemical Society Reviews* **2015**, *44*, 1379-1415.
102. Eliseeva, S.V.; Bünzli, J.-C.G. Lanthanide luminescence for functional materials and bio-sciences. *Chemical Society Reviews* **2010**, *39*, 189-227.
103. Kobayashi, H.; Ogawa, M.; Alford, R.; Choyke, P.L.; Urano, Y. New Strategies for Fluorescent Probe Design in Medical Diagnostic Imaging. *Chemical Reviews* **2010**, *110*, 2620-2640.
104. Nyk, M.; Kumar, R.; Ohulchanskyy, T.Y.; Bergey, E.J.; Prasad, P.N. High Contrast in Vitro and in Vivo Photoluminescence Bioimaging Using Near Infrared to Near Infrared Up-Conversion in Tm^{3+} and Yb^{3+} Doped Fluoride Nanophosphors. *Nano Letters* **2008**, *8*, 3834-3838.

105. Chen, C.; Wang, F.; Wen, S.; Su, Q.P.; Wu, M.C.L.; Liu, Y.; Wang, B.; Li, D.; Shan, X.; Kianinia, M., et al. Multi-photon near-infrared emission saturation nanoscopy using upconversion nanoparticles. *Nature Communications* **2018**, *9*, 3290.
106. Wang, C.; Cheng, L.; Liu, Z. Drug delivery with upconversion nanoparticles for multi-functional targeted cancer cell imaging and therapy. *Biomaterials* **2011**, *32*, 1110-1120.
107. Wang, F.; Wen, S.; He, H.; Wang, B.; Zhou, Z.; Shimoni, O.; Jin, D. Microscopic inspection and tracking of single upconversion nanoparticles in living cells. *Light: Science & Applications* **2018**, *7*, 18007-18007.
108. Rodríguez-Sevilla, P.; Zhang, Y.; Haro-González, P.; Sanz-Rodríguez, F.; Jaque, F.; Solé, J.G.; Liu, X.; Jaque, D. Thermal Scanning at the Cellular Level by an Optically Trapped Upconverting Fluorescent Particle. *Advanced Materials* **2016**, *28*, 2421-2426,.
109. Shen, J.; Zhao, L.; Han, G. Lanthanide-doped upconverting luminescent nanoparticle platforms for optical imaging-guided drug delivery and therapy. *Advanced Drug Delivery Reviews* **2013**, *65*, 744-755.
110. Li, X.; Zhang, F.; Zhao, D. Highly efficient lanthanide upconverting nanomaterials: Progresses and challenges. *Nano Today* **2013**, *8*, 643-676.
111. van der Ende, B.M.; Aarts, L.; Meijerink, A. Near-Infrared Quantum Cutting for Photovoltaics. *Advanced Materials* **2009**, *21*, 3073-3077.
112. Park, Y.I.; Kim, J.H.; Lee, K.T.; Jeon, K.-S.; Na, H.B.; Yu, J.H.; Kim, H.M.; Lee, N.; Choi, S.H.; Baik, S.-I., et al. Nonblinking and Nonbleaching Upconverting Nanoparticles as an Optical Imaging Nanoprobe and T1 Magnetic Resonance Imaging Contrast Agent. *Advanced Materials* **2009**, *21*, 4467-4471.
113. Chen, G.; Qiu, H.; Prasad, P.; Chen, X. Upconversion Nanoparticles: Design, Nanochemistry, and Applications in Theranostics. *Chemical reviews* **2014**, *114*, 5161–5214.
114. Shang, M.; Li, C.; Lin, J. How to produce white light in a single-phase host? *Chemical Society Reviews* **2014**, *43*, 1372-1386.
115. Lin, Y.-C.; Karlsson, M.; Bettinelli, M. Inorganic Phosphor Materials for Lighting. *Topics in Current Chemistry* **2016**, *374*.
116. Downing, E.; Hesselink, L.; Ralston, J.; Macfarlane, R. A Three-Color, Solid-State, Three-Dimensional Display. *Science* **1996**, *273*, 1185.
117. Tan, M.; del Rosal, B.; Zhang, Y.; Martín Rodríguez, E.; Hu, J.; Zhou, Z.; Fan, R.; Ortgies, D.H.; Fernández, N.; Chaves-Coira, I., et al. Rare-earth-doped fluoride nanoparticles with engineered long luminescence lifetime for time-gated in vivo optical imaging in the second biological window. *Nanoscale* **2018**, *10*, 17771-17780.
118. Naczynski, D.J.; Tan, M.C.; Zevon, M.; Wall, B.; Kohl, J.; Kulesa, A.; Chen, S.; Roth, C.M.; Riman, R.E.; Moghe, P.V. Rare-earth-doped biological composites as in vivo shortwave infrared reporters. *Nature Communications* **2013**, *4*, 2199.
119. Tian, G.; Gu, Z.; Liu, X.; Zhou, L.; Yin, W.; Yan, L.; Jin, S.; Ren, W.; Xing, G.; Li, S., et al. Facile Fabrication of Rare-Earth-Doped Gd2O3 Hollow Spheres with Upconversion Luminescence, Magnetic Resonance, and Drug Delivery Properties. *The Journal of Physical Chemistry C* **2011**, *115*, 23790-23796.
120. Shen, J.; Sun, L.-D.; Yan, C.-H. Luminescent rare earth nanomaterials for bioprobe applications. *Dalton Transactions* **2008**, 5687-5697.
121. Zhou, J.; Liu, Z.; Li, F. Upconversion nanophosphors for small-animal imaging. *Chemical Society Reviews* **2012**, *41*, 1323-1349.
122. Bouzigues, C.; Gacoin, T.; Alexandrou, A. Biological Applications of Rare-Earth Based Nanoparticles. *ACS Nano* **2011**, *5*, 8488-8505.
123. Zhou, J.; Sun, Y.; Du, X.; Xiong, L.; Hu, H.; Li, F. Dual-modality in vivo imaging using rare-earth nanocrystals with near-infrared to near-infrared (NIR-to-NIR) upconversion luminescence and magnetic resonance properties. *Biomaterials* **2010**, *31*, 3287-3295.
124. van Sark, W.G.; de Wild, J.; Rath, J.K.; Meijerink, A.; Schropp, R.E.I. Upconversion in solar cells. *Nanoscale Research Letters* **2013**, *8*, 81.

125. Lu, Y.; Zhao, J.; Zhang, R.; Liu, Y.; Liu, D.; Goldys, E.M.; Yang, X.; Xi, P.; Sunna, A.; Lu, J., et al. Tunable lifetime multiplexing using luminescent nanocrystals. *Nature Photonics* **2014**, *8*, 32-36.
126. Idris, N.M.; Jayakumar, M.K.G.; Bansal, A.; Zhang, Y. Upconversion nanoparticles as versatile light nanotransducers for photoactivation applications. *Chemical Society Reviews* **2015**, *44*, 1449-1478.
127. Liu, Y.; Lu, Y.; Yang, X.; Zheng, X.; Wen, S.; Wang, F.; Vidal, X.; Zhao, J.; Liu, D.; Zhou, Z., et al. Amplified stimulated emission in upconversion nanoparticles for super-resolution nanoscopy. *Nature* **2017**, *543*, 229-233.
128. Vetrone, F.; Naccache, R.; Zamarrón, A.; Juarranz de la Fuente, A.; Sanz-Rodríguez, F.; Martinez Maestro, L.; Martín Rodriguez, E.; Jaque, D.; García Solé, J.; Capobianco, J.A. Temperature Sensing Using Fluorescent Nanothermometers. *ACS Nano* **2010**, *4*, 3254-3258.
129. Qian, H.S.; Guo, H.C.; Ho, P.C.-L.; Mahendran, R.; Zhang, Y. Mesoporous-Silica-Coated Up-Conversion Fluorescent Nanoparticles for Photodynamic Therapy. *Small* **2009**, *5*, 2285-2290.
130. Yang, Y.; Shao, Q.; Deng, R.; Wang, C.; Teng, X.; Cheng, K.; Cheng, Z.; Huang, L.; Liu, Z.; Liu, X., et al. In Vitro and In Vivo Uncaging and Bioluminescence Imaging by Using Photocaged Upconversion Nanoparticles. *Angewandte Chemie International Edition* **2012**, *51*, 3125-3129.
131. van de Rijke, F.; Zijlmans, H.; Li, S.; Vail, T.; Raap, A.K.; Niedbala, R.S.; Tanke, H.J. Up-converting phosphor reporters for nucleic acid microarrays. *Nature Biotechnology* **2001**, *19*, 273-276.
132. Guo, H.; Sun, S. Lanthanide-doped upconverting phosphors for bioassay and therapy. *Nanoscale* **2012**, *4*, 6692-6706.
133. Bhargava, R.N.; Gallagher, D.; Hong, X.; Nurmikko, A. Optical properties of manganese-doped nanocrystals of ZnS. *Physical Review Letters* **1994**, *72*, 416-419.
134. Chen, W.; Joly, A.G.; Zhang, J.Z. Up-conversion luminescence of of Mn^{2+} ions in $Zn_{1-x}Mg_xS:Mn^{2+}$ nanoparticles. *Physical Review B* **2001**, *64*, 041202.
135. Chen, W.; Joly, A.; Malm, J.-O.; Bovin, J.-O. Upconversion luminescence of Eu^{3+} and Mn^{2+} in $ZnS:Mn^{2+}$, Eu^{3+} codoped nanoparticles. *Journal of Applied Physics* **2004**, *95*, 667-672.
136. Vetrone, F.; Boyer, J.-C.; Capobianco, J.A.; Speghini, A.; Bettinelli, M. Significance of Yb^{3+} concentration on the upconversion mechanisms in codoped $Y_2O_3:Er^{3+}$, Yb^{3+} nanocrystals. *Journal of Applied Physics* **2004**, *96*, 661-667.
137. Schäfer, H.; Ptacek, P.; Kömpe, K.; Haase, M. Lanthanide-Doped $NaYF_4$ Nanocrystals in Aqueous Solution Displaying Strong Up-Conversion Emission. *Chemistry of Materials* **2007**, *19*, 1396-1400.
138. Wu, S.; Han, G.; Milliron, D.; Aloni, S.; Altoe, M.V.; Talapin, D.; Cohen, B.; Schuck, P. Non-blinking and photostable upconverted luminescence from single lanthanide-doped nanocrystals. *Proceedings of the National Academy of Sciences of the United States of America* **2009**, *106*, 10917-10921.
139. Zhao, J.; Lu, Z.; Yin, Y.; McRae, C.; Piper, J.A.; Dawes, J.M.; Jin, D.; Goldys, E.M. Upconversion luminescence with tunable lifetime in $NaYF_4$:Yb,Er nanocrystals: role of nanocrystal size. *Nanoscale* **2013**, *5*, 944-952.
140. Suyver, J.F.; Aebischer, A.; García-Revilla, S.; Gerner, P.; Güdel, H.U. Anomalous power dependence of sensitized upconversion luminescence. *Physical Review B* **2005**, *71*, 125123.
141. Zhao, J.; Jin, D.; Schartner, E.P.; Lu, Y.; Liu, Y.; Zvyagin, A.V.; Zhang, L.; Dawes, J.M.; Xi, P.; Piper, J.A., et al. Single-nanocrystal sensitivity achieved by enhanced upconversion luminescence. *Nature Nanotechnology* **2013**, *8*, 729-734.
142. Gargas, D.J.; Chan, E.M.; Ostrowski, A.D.; Aloni, S.; Altoe, M.V.P.; Barnard, E.S.; Sanii, B.; Urban, J.J.; Milliron, D.J.; Cohen, B.E., et al. Engineering bright sub-10-nm upconverting nanocrystals for single-molecule imaging. *Nature Nanotechnology* **2014**, *9*, 300-305.
143. Wang, F.; Liu, X. Upconversion Multicolor Fine-Tuning: Visible to Near-Infrared Emission from Lanthanide-Doped $NaYF_4$ Nanoparticles. *Journal of the American Chemical Society* **2008**, *130*, 5642-5643.
144. Achatz, D.; Ali, R.; Wolfbeis, O. Luminescent Chemical Sensing, Biosensing, and Screening Using Upconverting Nanoparticles. *Topics in current chemistry* **2011**, *300*, 29-50.
145. Aebischer, A.; Hostettler, M.; Hauser, J.; Krämer, K.; Weber, T.; Güdel, H.; Buergi, h.-b. Structural and Spectroscopic Characterization of Active Sites in a Family of Light-Emitting Sodium Lanthanide Tetrafluorides. *Angewandte Chemie (International ed. in English)* **2006**, *45*, 2802-2806.

146. Liang, C.-H.; Teoh, L.-G.; Liu, K.; Chang, Y.-S. Near white light emission of BaY_2ZnO_5 doped with Dy^{3+} ions. *Journal of Alloys and Compounds* **2012**, *517*, 9–13.
147. Lai, H.; Bao, A.; Yang, Y.; Xu, W.; Tao, Y.; Yang, H. Preparation and luminescence property of Dy^{3+}-doped YPO_4 phosphors. *Journal of Luminescence* **2008**, *128*, 521-524.
148. Yi, G.S.; Chow, G.M. Synthesis of Hexagonal-Phase $NaYF_4$:Yb,Er and $NaYF_4$:Yb,Tm Nanocrystals with Efficient Up-Conversion Fluorescence. *Advanced Functional Materials* **2006**, *16*, 2324-2329.
149. Wisser, M.; Fischer, S.; Maurer, P.; Bronstein, N.; Chu, S.; Alivisatos, A.; Salleo, A.; Dionne, J. Enhancing Quantum Yield via Local Symmetry Distortion in Lanthanide-Based Upconverting Nanoparticles. *ACS Photonics* **2016**, *3*.
150. Chan, E.M. Combinatorial approaches for developing upconverting nanomaterials: high-throughput screening, modeling, and applications. *Chemical Society Reviews* **2015**, *44*, 1653-1679.
151. Tu, L.; Liu, X.; Wu, F.; Zhang, H. Excitation energy migration dynamics in upconversion nanomaterials. *Chemical Society Reviews* **2015**, *44*, 1331-1345.
152. Zhang, W.; Xie, P.; Duan, C.; Yan, K.; Yin, M.; Lou, L.; Xia, S.; Krupa, J.-C. Preparation and size effect on concentration quenching of nanocrystalline Y_2SiO_5:Eu. *Chemical Physics Letters* **1998**, *292*, 133-136.
153. Flores-Gonzalez, M.A.; Ledoux, G.; Roux, S.; Lebbou, K.; Perriat, P.; Tillement, O. Preparing nanometer scaled Tb-doped Y_2O_3 luminescent powders by the polyol method. *Journal of Solid State Chemistry* **2005**, *178*, 989-997.
154. Collins, J. Non-Radiative Processes in Crystals and in Nanocrystals. *ECS Journal of Solid State Science and Technology* **2015**, *5*, R3170-R3184 and references therein
155. Schietinger, S.; Menezes, L.d.S.; Lauritzen, B.; Benson, O. Observation of Size Dependence in Multicolor Upconversion in Single Yb^{3+}, Er^{3+} Codoped $NaYF_4$ Nanocrystals. *Nano Letters* **2009**, *9*, 2477-2481.
156. Liu, G.K.; Zhuang, H.Z.; Chen, X.Y. Restricted Phonon Relaxation and Anomalous Thermalization of Rare Earth Ions in Nanocrystals. *Nano Letters* **2002**, *2*, 535-539
157. Macedo, A.G.; Ferreira, R.A.S.; Ananias, D.; Reis, M.S.; Amaral, V.S.; Carlos, L.D.; Rocha, J. Effects of Phonon Confinement on Anomalous Thermalization, Energy Transfer, and Upconversion in Ln^{3+}-Doped Gd_2O_3 Nanotubes. *Advanced Functional Materials* **2010**, *20*, 624-634.
158. Boyer, J.-C.; van Veggel, F.C.J.M. Absolute quantum yield measurements of colloidal $NaYF_4$: Er^{3+}, Yb^{3+} upconverting nanoparticles. *Nanoscale* **2010**, *2*, 1417-1419.
159. Johnson, N.J.J.; He, S.; Diao, S.; Chan, E.M.; Dai, H.; Almutairi, A. Direct Evidence for Coupled Surface and Concentration Quenching Dynamics in Lanthanide-Doped Nanocrystals. *Journal of the American Chemical Society* **2017**, *139*, 3275-3282.
160. Haase, M.; Schäfer, H. Upconverting Nanoparticles. *Angewandte Chemie International Edition* **2011**, *50*, 5808-5829.
161. Chen, G.; Yang, C.; Prasad, P.N. Nanophotonics and Nanochemistry: Controlling the Excitation Dynamics for Frequency Up- and Down-Conversion in Lanthanide-Doped Nanoparticles. *Accounts of Chemical Research* **2013**, *46*, 1474-1486.
162. Wang, X.; Yan, X.H.; Kan, C.; Ma, K.; Xiao, Y.; Xiao, S. Enhancement of blue emission in β -$NaYbF_4$:Tm^{3+} /Nd^{3+} nanophosphors synthesized by nonclosed hydrothermal synthesis method. *Applied Physics B-lasers and Optics - APPL PHYS B-LASERS OPT* **2010**, *101*, 623-629
163. Dong, C.; Pichaandi, J.; Regier, T.; van Veggel, F.C.J.M. Nonstatistical Dopant Distribution of Ln^{3+}-Doped $NaGdF_4$ Nanoparticles. *The Journal of Physical Chemistry C* **2011**, *115*, 15950-15958.
164. Cojocaru, B.; Avram, D.; Kessler, V.; Parvulescu, V.; Seisenbaeva, G.; Tiseanu, C. Nanoscale insights into doping behavior, particle size and surface effects in trivalent metal doped SnO_2. *Scientific Reports* **2017**, *7*, 9598
165. Yang, P.; Deng, P.; Yin, Z. Concentration quenching in Yb:YAG. *Journal of Luminescence* **2002**, *97*, 51-54.
166. Viger, M.L.; Live, L.S.; Therrien, O.D.; Boudreau, D. Reduction of Self-Quenching in Fluorescent Silica-Coated Silver Nanoparticles. *Plasmonics* **2008**, *3*, 33-40.

167. Wang, Y.-F.; Liu, G.-Y.; Sun, L.-D.; Xiao, J.-W.; Zhou, J.-C.; Yan, C.-H. Nd^{3+}-Sensitized Upconversion Nanophosphors: Efficient In Vivo Bioimaging Probes with Minimized Heating Effect. *ACS Nano* **2013**, *7*, 7200-7206.
168. Wang, F.; Deng, R.; Wang, J.; Wang, Q.; Han, Y.; Zhu, H.; Chen, X.; Liu, X. Tuning upconversion through energy migration in core–shell nanoparticles. *Nature Materials* **2011**, *10*, 968-973 and references therein.
169. Zhong, Y.; Tian, G.; Gu, Z.; Yang, Y.; Gu, L.; Zhao, Y.; Ma, Y.; Yao, J. Elimination of Photon Quenching by a Transition Layer to Fabricate a Quenching-Shield Sandwich Structure for 800 nm Excited Upconversion Luminescence of Nd^{3+}-Sensitized Nanoparticles. *Advanced Materials* **2014**, *26*, 2831-2837.
170. Wen, H.; Zhu, H.; Chen, X.; Hung, T.F.; Wang, B.; Zhu, G.; Yu, S.F.; Wang, F. Upconverting Near-Infrared Light through Energy Management in Core–Shell–Shell Nanoparticles. *Angewandte Chemie International Edition* **2013**, *52*, 13419-13423.
171. Deng, R.; Qin, F.; Chen, R.; Huang, W.; Hong, M.; Liu, X. Temporal full-colour tuning through non-steady-state upconversion. *Nature Nanotechnology* **2015**, *10*, 237-242.
172. Chen, G.; Ågren, H.; Ohulchanskyy, T.Y.; Prasad, P.N. Light upconverting core–shell nanostructures: nanophotonic control for emerging applications. *Chemical Society Reviews* **2015**, *44*, 1680-1713.
173. DiMaio, J.R.; Kokuoz, B.; James, T.; Ballato, J. Structural Determination of Light-Emitting Inorganic Nanoparticles with Complex Core/Shell Architectures. *Advanced Materials* **2007**, *19*, 3266-3270.
174. Zhou, B.; Tang, B.; Zhang, C.; Qin, C.; Gu, Z.; Ma, Y.; Zhai, T.; Yao, J. Enhancing multiphoton upconversion through interfacial energy transfer in multilayered nanoparticles. *Nature Communications* **2020**, *11*, 1174.
175. Jares-Erijman, E.A.; Jovin, T.M. FRET imaging. *Nature Biotechnology* **2003**, *21*, 1387-1395.
176. Sun, T.; Ma, R.; Qiao, X.; Fan, X.; Wang, F. Shielding Upconversion by Surface Coating: A Study of the Emission Enhancement Factor. *ChemPhysChem* **2016**, *17*, 766-770.
177. Wilhelm, S. Perspectives for Upconverting Nanoparticles. *ACS Nano* **2017**, *11*, 10644-10653.
178. Liu, X.; Yan, C.-H.; Capobianco, J.A. Photon upconversion nanomaterials. *Chemical Society Reviews* **2015**, *44*, 1299-1301.
179. Kömpe, K.; Borchert, H.; Storz, J.; Lobo, A.; Adam, S.; Möller, T.; Haase, M. Green-Emitting $CePO_4$:Tb/$LaPO_4$ Core–Shell Nanoparticles with 70 % Photoluminescence Quantum Yield. *Angewandte Chemie International Edition* **2003**, *42*, 5513-5516.
180. Qian, H.-S.; Zhang, Y. Synthesis of Hexagonal-Phase Core−Shell $NaYF_4$ Nanocrystals with Tunable Upconversion Fluorescence. *Langmuir* **2008**, *24*, 12123-12125.
181. Chen, G.; Damasco, J.; Qiu, H.; Shao, W.; Ohulchanskyy, T.Y.; Valiev, R.R.; Wu, X.; Han, G.; Wang, Y.; Yang, C., et al. Energy-Cascaded Upconversion in an Organic Dye-Sensitized Core/Shell Fluoride Nanocrystal. *Nano Letters* **2015**, *15*, 7400-7407.
182. Wang, X.; Valiev, R.R.; Ohulchanskyy, T.Y.; Ågren, H.; Yang, C.; Chen, G. Dye-sensitized lanthanide-doped upconversion nanoparticles. *Chemical Society Reviews* **2017**, *46*, 4150-4167.
183. Wu, D.M.; García-Etxarri, A.; Salleo, A.; Dionne, J.A. Plasmon-Enhanced Upconversion. *The Journal of Physical Chemistry Letters* **2014**, *5*, 4020-4031.
184. Park, W.; Lu, D.; Ahn, S. Plasmon enhancement of luminescence upconversion. *Chemical Society Reviews* **2015**, *44*, 2940-2962.
185. Glass, A.M.; Liao, P.F.; Bergman, J.G.; Olson, D.H. Interaction of metal particles with adsorbed dye molecules: absorption and luminescence. *Optics Letters* **1980**, *5*, 368-370.
186. Lakowicz, J.R. Radiative Decay Engineering: Biophysical and Biomedical Applications. *Analytical Biochemistry* **2001**, *298*, 1-24.
187. Dulkeith, E.; Morteani, A.C.; Niedereichholz, T.; Klar, T.A.; Feldmann, J.; Levi, S.A.; van Veggel, F.C.J.M.; Reinhoudt, D.N.; Möller, M.; Gittins, D.I. Fluorescence Quenching of Dye Molecules near Gold Nanoparticles: Radiative and Nonradiative Effects. *Physical Review Letters* **2002**, *89*, 203002.
188. Saboktakin, M.; Ye, X.; Oh, S.J.; Hong, S.-H.; Fafarman, A.T.; Chettiar, U.K.; Engheta, N.; Murray, C.B.; Kagan, C.R. Metal-enhanced upconversion luminescence tunable through metal nanoparticle-nanophosphor separation. *ACS nano* **2012**, *6*, 8758-8766.

189. Schietinger, S.; Aichele, T.; Wang, H.-Q.; Nann, T.; Benson, O. Plasmon-enhanced upconversion in single $NaYF_4$:Yb^{3+}/Er^{3+} codoped nanocrystals. *Nano letters* **2010**, *10*, 134-138.
190. Greybush, N.J.; Saboktakin, M.; Ye, X.; Della Giovampaola, C.; Oh, S.J.; Berry, N.E.; Engheta, N.; Murray, C.B.; Kagan, C.R. Plasmon-Enhanced Upconversion Luminescence in Single Nanophosphor–Nanorod Heterodimers Formed through Template-Assisted Self-Assembly. *ACS Nano* **2014**, *8*, 9482-9491.
191. Bang, D.; Jo, E.-J.; Hong, S.; Byun, J.-Y.; Lee, J.Y.; Kim, M.-G.; Lee, L.P. Asymmetric Nanocrescent Antenna on Upconversion Nanocrystal. *Nano Letters* **2017**, *17*, 6583-6590.
192. Saboktakin, M.; Ye, X.; Chettiar, U.K.; Engheta, N.; Murray, C.B.; Kagan, C.R. Plasmonic Enhancement of Nanophosphor Upconversion Luminescence in Au Nanohole Arrays. *ACS Nano* **2013**, *7*, 7186-7192.
193. Wang, F.; Liu, X. Multicolor Tuning of Lanthanide-Doped Nanoparticles by Single Wavelength Excitation. *Accounts of Chemical Research* **2014**, *47*, 1378-1385.
194. George, N.C.; Denault, K.; Seshadri, R. Phosphors for Solid-State White Lighting. *Annual Review of Materials Research* **2013**, *43*, 481-501 and references therein.
195. Meltzer, R.S.; Feofilov, S.P.; Tissue, B.; Yuan, H.B. Dependence of fluorescence lifetimes of of Y_2O_3:Eu^{3+} nanoparticles on the surrounding medium. *Physical Review B* **1999**, *60*, R14012-R14015.
196. Schniepp, H.; Sandoghdar, V. Spontaneous Emission of Europium Ions Embedded in Dielectric Nanospheres. *Physical Review Letters* **2002**, *89*, 257403
197. Benner, R.E.; Barber, P.W.; Owen, J.F.; Chang, R.K. Observation of Structure Resonances in the Fluorescence Spectra from Microspheres. *Physical Review Letters* **1980**, *44*, 475-478.
198. Reid, M. F.; *Crystal Field Handbook*; Newman, D.J., Ng, B., Eds.; Cambridge University Press: Cambridge, **2000**, pp 190–226.
199. Condon, E. U.; Shortley, G. H. The Theory of Atomic Spectra. New York: Cambridge Univ. Press, 1951.
200. Albrecht, C. Joseph R. Lakowicz: Principles of fluorescence spectroscopy, 3rd Edition. *Analytical and Bioanalytical Chemistry* **2008**, *390*, 1223-1224.
201. McCumber, D.E.; Sturge, M.D. Linewidth and Temperature Shift of the R Lines in Ruby. *Journal of Applied Physics* **1963**, *34*, 1682-1684.
202. Hong, K.S.; Yang, I.H.-S. Electron-phonon interactions in insulating nanoparticles Eu_2O_3. *Journal of the Korean Physical Society* **2005**, *47*, S200-S203.
203. Tamura, A. Smoothed density of states of electrons and smoothed frequency spectrum of phonons for a mesoscopic system. *Physical Review B* **1995**, *52*, 2668-2677.
204. Liu, G. A degenerate model of vibronic transitions for analyzing 4f–5d spectra. *Journal of Luminescence* **2014**, *152*, 7-10.
205. Zhou, X.; Tanner, P.A.; Faucher, M.D. Electronic Spectra and Crystal Field Analysis of Er^{3+} in Cs_2NaErF_6. *The Journal of Physical Chemistry C* **2007**, *111*, 683-687.
206. Chen, X.; Di Bartolo, B.; Barnes, N.; Walsh, B. Thermal tuning and broadening of the spectral lines of trivalent neodymium in laser crystals. *physica status solidi (b)* **2004**, *241*, 1957-1976.
207. Yang, H.-S.; Feofilov, S.P.; Williams, D.K.; Milora, J.C.; Tissue, B.M.; Meltzer, R.S.; Dennis, W.M. One phonon relaxation processes in Y2O3 : Eu3+ nanocrystals. *Physica B: Condensed Matter* **1999**, *263-264*, 476-478.
208. Tamura, A.; Ichinokawa, T. Frequency spectrum of a small particle. *Journal of Physics C: Solid State Physics* **1983**, *16*, 4779-4788.
209. Chen, X.Y.; Zhuang, H.Z.; Liu, G.K.; Li, S.; Niedbala, R.S. Confinement on energy transfer between luminescent centers in nanocrystals. *Journal of Applied Physics* **2003**, *94*, 5559-5565.
210. Wang, Y.; Xu, W.; Yongsheng, Z.; Xu, S.; Cui, H.; Song, H. Phonon-modulated upconversion luminescence properties in some Er^{3+} and Yb^{3+} co-activated oxides. *J. Mater. Chem. C* **2014**, *2*.
211. Liu, G.; Chen, X.; Zhuang, H.; Li, S.; Niedbala, R. Confinement of electron-phonon interaction on luminescence dynamics in nanophosphors of Er3+:Y2O2S. *Journal of Solid State Chemistry - J SOLID STATE CHEM* **2003**, *171*, 123-1320.

212. Stouwdam, J.W.; van Veggel, F.C.J.M. Near-infrared Emission of Redispersible Er^{3+}, Nd^{3+}, and Ho^{3+} Doped LaF_3 Nanoparticles. *Nano Letters* **2002**, *2*, 733-737q.
213. Wang, W.; Liu, G.K.; Brik, M.G.; Seijo, L.; Shi, D. 5s-6d orbital hybridization of trivalent uranium in crystals of hexagonal symmetry: Effects on electronic energy levels and transition intensities. *Physical Review B* **2009**, *80*, 155120.
214. Hreniak, D.; Stręk, W.; Głuchowski, P.; Bettinelli, M.; Speghini, A. The influence of the specific surface of grains on the luminescence properties of Nd^{3+}-doped $Y_3Al_5O_{12}$ nanopowders. *Applied Physics B* **2008**, *91*, 89-93.
215. Otsuka, K.; Yamada, T.; Saruwatari, M.; Kimura, T. Spectroscopy and Laser Oscillation Properties of Lithium Neodymium Tetraphospnate. *Quantum Electronics, IEEE Journal of* **1975**, *QE-11*, 330-335.
216. Marciniak, L.; Stefanski, M.; Tomala, R.; Hreniak, D.; Strek, W. Size effect in luminescent properties of $LiNdP_4O_{12}$ nanocrystals. *Optical Materials* **2015**, *41*, 17-20.
217. Wiglusz, R.J.; Marciniak, L.; Pazik, R.; Strek, W. Structural and Spectroscopic Characterization of Nd^{3+}-Doped YVO_4 Yttrium Orthovanadate Nanocrystallites. *Crystal Growth & Design* **2014**, *14*, 5512-5520.
218. Strek, W.; Marciniak, L.; Bednarkiewicz, A.; Lukowiak, A.; Hreniak, D.; Wiglusz, R. The effect of pumping power on fluorescence behavior of $LiNdP_4O_{12}$ nanocrystals. *Optical Materials* **2011**, *33*, 1097-1101.